Wesleyan University The Honors Program

THE CONTINUED DEVELOPMENT OF A SCANNING TUNNELING MICROSCOPE AND A PRELIMINARY INVESTIGATION OF THE TOPOGRAPHY OF EVAPORATED Au THIN FILMS ON GLASS

by
Daryl Tulimieri

Class of 1993

A thesis submitted to the
Faculty of Wesleyan University
in partial fulfillment of the requirements for the
Degree of Bachelor of Arts
with Departmental Honors in the Department of Physics

Middletown, Connecticut April,1993

ACKNOWLEDGEMENTS

First I would like to thank my advisor Fred Ellis for taking a chance by letting a freshman into his lab three years ago. And besides the thanks for being an inexhaustible fountain of knowledge in any area of physics, I would like to express my gratitude to him for encouraging me to pursue interests outside of physics and then waiting patiently while I took his advice to extremes.

I cannot express enough gratitude to my parents whose support has never faltered over the years despite my concerted efforts to make it as difficult as possible. There has never been two more selfless people. Thank you for letting me be an adult.

Finally, I would like to thank Riina Delta Tehver for providing the inspiration and justification for all of this and for never letting me stop thinking.

TABLE OF CONTENTS

ABSTRACT

Part I of this thesis is an evaluation of the scanning tunneling microscope and its present condition. Difficulties with its operation are discussed and various solutions presented. The section is intended to build on the experience of Bill Cahill and Jason Firing who worked on the present STM and also on the earlier work of those who laid the foundation for this project. Recommendations are made to facilitate the continued development of the microscope.

In Part II the reliability of data provided by the STM is discussed. The data are compared with previously reported data and are determined to be valid with a fair amount of confidence. Using this information a preliminary characterization of the topography of evaporated gold films on glass is presented

PART I: THE STM

Since the development of the first scanning tunneling microscope (STM) by Binnig and Rohrer in 1982[1] many different designs and variations have been investigated. The simple operating principles of a STM, and the fact that commercial STM's remain costly, has encouraged many laboratories interested in scanning tunneling microscopy (also STM) to design and build their own microscopes.

The basis of the operation is the quantum mechanical tunnel effect. The tunnel junction consists of a sharp tip which is brought to close proximity with a conducting surface until the electron quantum wave functions in the tip and in the surface are able to tunnel across the potential barrier between the two. A bias voltage is placed on the tip to create a net flow of electrons in one direction - the tunneling current. This current is highly dependent upon the separation of the tip and surface varying exponentially with the separation[2]. The tip is scanned across the surface in a raster pattern while being kept at a constant distance from the surface by monitoring the tunneling current. The motion of the tip required to maintain a constant current is recorded, effectively reproducing the topology of the surface.

Almost all STMs and probe microscopes[3] use ceramic

piezoelectric micropositioners. These materials respond to electric fields by expanding or contracting dependant upon the orientation of the polarization of the material relative to the field. Their motion is accurate on a sub-angstrom level. The tunneling junction (in STM) is maintained by a feedback mechanism which applies voltages to the piezoelectric to follow the surface.

Here I will discuss the layout of our microscope concentrating on these elements and its virtues and drawbacks will be outlined. Suggestions will also be made for improving the microscope design. Part I of this thesis is intended to be useful for students continuing work on the STM. For this reason considerable attention is paid to supplying practical information for the use, modification, and eventual redesign of the microscope.

CHAPTER I: THE APPARATUS

The present state of the body of the microscope is examined. Emphasis is on suggestions for improvements for a new STM concentrating on the actuator design and performance.

THE ACTUATOR

The actuator of this STM is a novel one. Its originality stems from its shape and method by which it produces orthogonal motion in three dimensions. A cross was cut from a piezoelectric wafer with four equal arms. The piezoelectric is a bimorph in which two ceramic layers sandwich a brass electrode and the outer surfaces are both plated with nickel. This nickel plating is etched so that the four arms are electrically isolated from each other on both sides. The tip is mounted on a square isolated portion of the actuator located where the arms of the crosspiece intersect. The arrangement is shown in Figure 1.

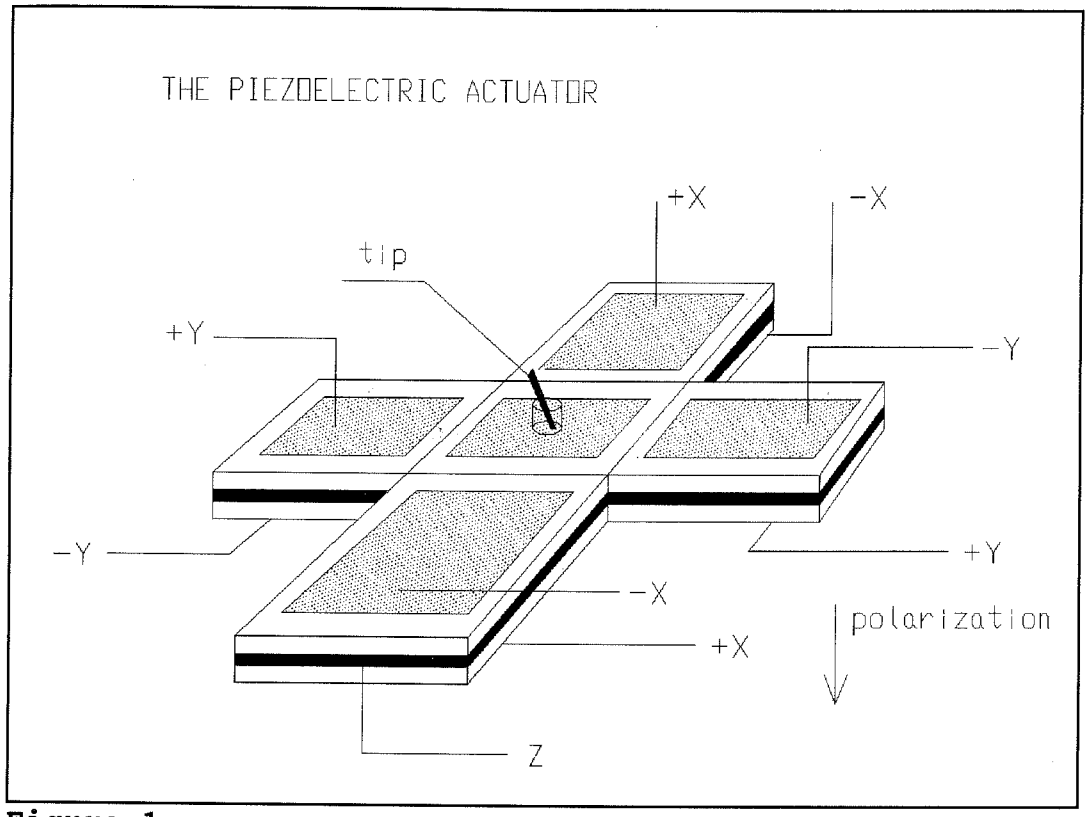

Figure 1

X, Y, AND Z MOTION

The X and Y (lateral, or horizontal) motion are produced by applying a balanced signal to opposite faces of each arm. For example, representing the center of the crosspiece as the origin, the arm in the +X direction has a positive signal on the top nickel electrode and a balanced negative signal on the bottom electrode. The arm extending in the -X direction has the positive voltage applied to the bottom electrode and the balanced negative signal applied to the top electrode. The arms

are polarized in the same direction so that when the voltage causes one arm to contract it causes the other arm to expand by the same distance. The same is done in the y direction. This combination allows simultaneous unrestricted motion in the plane parallel to the surface being scanned with a maximum range of about 400 nm in the X direction and 800 nm in the Y direction. Excellent detailed descriptions of this motion are available in honors theses by Cahill[4] and Firing[5].

Motion in the Z (vertical) direction is created in a different manner. When a voltage is applied to central brass electrode the electric field in the piezoelectric between this electrode and the nickel electrodes is altered. The entire ceramic layer above the electrode will either expand or contract and the entire ceramic layer below the electrode will have the opposite reaction. The layers are glued together, so this asymmetry causes a buckling of the bimorph much like a heated bi-metal strip. The motion of the piezoelectric is on a nanometer scale, so it is assumed that a first order approximation for the displacement of the tip as a function of the applied voltages is valid. That is, the motion is linear in X, Y, and Z. This approximation has been validated by repeated calibrations of the motion by myself, Firing, and Cahill.

ADVANTAGES AND DISADVANTAGES

There are several advantages to this approach to the motion of the tip. The first is that the effective range of the STM in the Z direction is very large compared to the size of the actuator. The vertical sensitivity of the crosspiece is 120 Å/V, giving a range of nearly 2500 nm. While ranges of this size are achieved by other configurations, ours seems to have substantially less drift than that described by researchers using other designs. This drift can be caused by thermal expansion of the body of the STM or by a drifting of the response of the piezoelectric itself when in a voltage potential[6]. Also, since it is one piece, the actuator is sturdy and easily mounted.

There are also disadvantages to the configuration. One inherent difficulty is that of the close proximity of the electrical contacts. The control voltages come from a receptor plug mounted on the body of the STM. There are five wires which lead into a cramped area where the crosspiece is located. The two balanced signals for the X and Y motion, four conductors, must be brought to the faces of the crosspiece at two sites each, eight contacts. The Z voltage, mercifully, must only be connected in one place to the brass electrode.

While this is easily done on a circuit board,

bringing the wires into a small area not much larger than a square centimeter poses a number of problems. The wires must each be secured to one face and then to the opposite face of the bimorph on the opposite arm. In this manner the wires crisscross in a number of places in an even smaller awkwardly accessed area. They also must be kept from contacting the bimorph when they are bent around it. The size of the area, the fact that the wires must be connected at more than one site each, and the desire to reduce forces and vibrations on the actuator make it convenient to use very small non-insulated wires. There are simply too many opportunities for each wire to touch something it shouldn't, i.e. another wire, a contact, or ground.

This is an inherent problem with the present design that should be addressed if the STM makes another evolutionary lunge. One solution might be to run insulated or coaxial leads from a plug and permanently mount each of them in close proximity to the electrode that it must contact. This would involve twice as many leads in order to run the four signals separately to the top and bottom sides of the bimorph, but with insulated leads and a more accessible design this may prove more reliable that the present configuration. Otherwise, alternative designs may be considered such as the tube design discussed in the next section.

The motion of the actuator in any direction is dependent upon the reaction of several distinct sections of the bimorph. This makes the design susceptible to mechanical coupling, so that the movement in the three directions is not entirely orthogonal. This is also present with other designs[7], but it unclear to what extent.

And while the motion in the Z direction is large, the range in the horizontal directions is comparable to only the shortest ranges available on commercial STMs. The range is less, but the response of the design, approximately 20 Å/V in X and 40 Å/V in Y, is about average. The difference is also in the high voltage amplifiers generally used. Most are capable of anywhere from ±150 V to ±400 V compared to our ±100 V amplifier. In practice this has not yet been a limiting factor.

ALTERNATIVES

In order to ascertain the true value of these ranges I compared them to the specifications of one of the most popular commercial STMs, the Nanoscope II™. They employ the "tube" design, described below, and maximize the total range of the instrument by making the actuator, or "scanner" as they refer to it, easily replaceable. There are four scanners available with horizontal sensitivities

of 20, 35, 100, and 300 Å/V, and respective vertical sensitivities of 20, 30, 40, and 100 Å/V. This gives our crosspiece a horizontal range equal to that of their smallest scanner and a vertical range larger than that of their largest scanner.

Two common alternatives are the "tube" design and the "orthogonal configuration" design[8]. In the tube design the inner and outer faces of a hollow piezoelectric cylinder are coated with a conducting material to serve as electrodes. The outer face is divided parallel to the axis of symmetry of the cylinder into 4 equal sections. Balanced signals are sent to quarters opposite each other to cause the tube to bend in the X and Y direction. The Z motion is achieved by changing the potential of the inner face, which is common to the whole tube, changing the potential across each section equally. This way the length of the tube is increased or decreased without changing the X and Y positions.

The second design is very simple. Three separate piezoelectric transducers are mounted mutually orthogonal and meet at a common vertex. Voltages are applied to each to produce simple expansion along each axis. A boring approach compared to the others, but also an effective one.

THE TIP

The most basic operating principle of STM is of course the tunneling junction, i.e. the tip/surface junction. In this sense the tip is the most critical part of the entire instrument. It is ultimately the tip that determines the highest possible resolution attainable. For this reason, great care must be taken in fashioning STM tips.

Our tips are fabricated from Pt, 0.001 cm monofilament commercially available from Englehard Corporation. The filament is stored in a highly isolated polypropylene containment device in a carefully controlled aerostatic environment held at precisely 7.4×10^2 Torr, 291 K, with a gaseous content of 78% N, 21% O and approximate relative aqueous content of 20%, where it remains indefinitely stable until needed. The sample is machined using an Fe cutting tool acquired from Precision Blades Unlimited on a macroscopically flat Al surface to a length of 2×10^3 μ. A set of precision stainless steel forceps are used under an optical microscope to position the tip.

The tip is connected to the feedback loop by a mini-coaxial cable which is shielded to within 1 mm of the tip in order to reduce electromagnetic pickup. The coax also acts as a spring, exerting a constant force on the tip,

holding it in place on the actuator.

Although the data gathered by the STM are reliable in their reproducibility, some question remains as to how they should be interpreted. One major factor is contamination. This was a central theme of the thesis by Cahill. Another aspect is the tip. There is no way of knowing what the tip looks like on the atomic scale important to its function as a tunneling probe. The easiest, and possibly only, way to determine the sharpness of the tip is to calculate a resolution based on scanning a known surface structure. In STM this is routinely done by scanning the fcc structure of cleaved graphite with atomic resolution. Although several attempts were made, I was unable to get a reliable scan of graphite for this purpose. A concerted effort should be made to accomplish this as it will also give a much better calibration of the microscope than the methods presently used.

I also came across a method of effective tip change described by Emch et al.[9], but was not able to implement any such device. It involves applying a voltage pulse directly to the tip, not to the feedback loop, on the order of a few volts for 10 - 100 ns while the tip was tunneling. This apparently induces a discharge from the tip which cleans and reshapes the tip. It also has the mixed blessing of creating a hole in the surface of the

surface of the gold substrate. Destroying the features of the surface you want to characterize is not entirely productive, but this has been used widely as a lithographic technique to write nanometer scale features onto surfaces as well as to fix foreign atoms to the surface[10]. Pulses of 5 V produced "massive tip changes," presumably meaning that the tunneling junction moved to an entirely different region of the tip. This should be easily implemented by way of the bias adjust leading to the tip.

THE OBSTACLES

There is a serious problem of occasional uncontrollable, very high frequency, large amplitude oscillations. This will be discussed further along with the description of the electronic feedback mechanism, but the problem may also stem from the physical properties of the piezoelectric. More specifically, the large range of the Z actuator, while a theoretical asset to the design, may make it too unstable. There are also obstacles making it difficult to correct this. If the polarization is reduced to make the actuator more rigid in the Z direction, the X and Y ranges are also reduced. It could be possible to put a physical force on the actuator to stiffen it. Designing such a device to restrict the

motion is not only difficult but poses the risk of introducing more vibrational noise almost directly to the tip.

In theory our design compares favorably to the others mentioned given its size and specifications, even more so if one considers that the crosspiece runs at lower voltages than most other actuators. Thus far the range of the crosspiece itself has not been a limiting factor at all. The susceptibility of the Z positioner to the oscillations described above is largely dependent upon the overall gain of the feedback loop. The higher the gain, the more likely it is that oscillations will occur. They do not seem to get worse with aging of the tip or of the substrate and were present even with gold films exposed to air less than an hour. They may still be due to contaminants on the surface, although most studies of gold are done in air without this problem.

This has limited the Z range exploitable under feedback conditions to no more than 50 nm. The most successful scans were done in conditions where the feedback range was about 20 nm. While none of the individual features observed were larger than this, it proved difficult to keep the surface within tunneling range over long distances. This is due to a combination of possible non-horizontal positioning of the sample, changes in film thickness, non-linear coupling of the X,

The sample was kept flat mainly by making sure that the area where it is mounted was kept free of dirt and by securing it well to the holder. The change in thickness of the gold film was precisely what we were looking to measure, so this was not something to be eliminated at all.

Thermal drift was a topic covered in detail by Cahill and he considered it to be a significant obstacle that needed to be overcome before successful imaging would be possible. I found one rather simple solution to the problem of thermal drift: patience. The amount of drift logically depended on how much the STM had been moved or handled, hence changing its temperature. This was especially true if it had been under an optical microscope that uses a high intensity lamp for illumination. This was the case when changing tips. It could take from one to six hours to achieve stability. The STM was typically allowed to "cool down" overnight before scanning, but this was usually not necessary. Once the tip had been brought within tunneling range while the microscope was in equilibrium, the surface usually remained within range of the piezodrive indefinitely, at least on the order of weeks.

The final concern aggravating this limitation is coupling between the horizontal and vertical motions of the actuator. This coupling was first described by

the actuator. This coupling was first described by Firing[11]. The coupling is qualitatively different in the X and Y directions. In the X direction it is almost perfectly linear. Firing reported a slope of about -0.1 on a flat surface, and I recorded a slope only slightly larger. Also in agreement with Firing, the Y coupling is more erratic. Under extreme negative voltages there is a slope of -0.15 and under extreme positive voltages a slope of less than 0.07. The transition between these slopes is smooth with little or no slope around 0 V. Correction of the vertical horizontal coupling will be discussed along with the feedback circuitry. If another crosspiece is constructed a primary concern is that it be machined as precisely as possible to reduce this coupling. All actuators have some amount of coupling and the correction is typically made in the display software.

The piezoelectric actuator is surely the most critical element of the STM apparatus, but other elements are also among the obstacles encountered in scanning a sample. The two other mechanical elements are the coarse and find adjustments for positioning the sample and the tip within range of the piezoelectric. The sample is mounted on a piston connected directly to a standard micrometer, the coarse adjust. The actuator is mounted on a cantilever arm that is machined out of the aluminum block that makes up the body of the microscope. This

cantilever arm is connected to a micrometer by a spring thereby applying a varying force to the cantilever arm bending it to alter its position, the fine adjust.

While these positioners are effective, they also have drawbacks. The first is that they are completely mechanical making it necessary to touch the microscope in order to adjust them. This upsets the spring suspended vibration suppression table (an iron machining table ≈200 kg) on which the microscope rests. It can take ½ hour for the residual vibrations of the table to subside to acceptable levels. Also, the spring and cantilever arm surely act as vibrational noise antennas for the tip. Even though the STM is enclosed in an aluminum box on the table, speaking in a normal voice while the tip is tunneling can still result in vibrations of the tip as large as a nanometer.

Despite the difficulties inherent in the design of this novel actuator, it is functional as an STM micropositioner. The successful imaging of gold surfaces and acquisition of useful data on the nanometer scale are the most convincing arguments in support of this claim. There are, of course, improvements to be made. The main obstacle to improved operation of the STM is the presence of the signal oscillations described above. If modifications to the apparatus and to the feedback and control mechanisms cannot significantly reduce these

oscillations, I would recommend replacing the crosspiece with a tube scanner. It seems to be more reliable than the orthogonal configuration. I recommend this only as a last resort, the same performance should be available from the crosspiece.

Now that the STM is computer controlled, the mechanical micropostioners should be updated. There are several ways this can be done. One is with a very large range piezoelectric positioner. I do not recommend this because it is unlikely to entirely eliminate the need for a mechanical positioner and also because these piezoelectrics are known to drift substantially. Another is the "rail" system. The sample holder is placed on a set of rails that nudge the holder forward using a sawtooth vibration, a stick/slip effect. The third is a micrometer controlled by a stepper motor. Either of the latter two should be able to advance the sample in increments of 50 nm or less toward the tip. If the STM is operating properly this step size will be well within the range of the feedback capabilities. The actuator can then be mounted to a rigid part of the STM body, which, in turn, can be made smaller, raising resonant frequencies and reducing vibrational noise yet further.

CHAPTER II: THE CONTROL HARDWARE

The control hardware is described in detail. Essential knowledge about the system is presented, difficulties are discussed and suggestions for improvements are made.

A critical part of the STM is the system used to control the voltages that drive the tip. This system consists of several parts: the high voltage driver, the feedback circuitry, and the computer. These circuits control three distinct data streams, one for each axis of motion. I will discuss the limitations that this imposes on the operation. Over the past three years the physical design of the STM has not changed at all, but improvements in the electronics controlling the STM alone have brought it from being an experiment itself, to a functional instrument capable of providing valuable data of surface topography. This emphasizes the importance of the control system.

3-D MOTION

The horizontal motion, X and Y, is controlled by the computer interfaced to the high voltage driver through a Data Translations DT2801 DA/AD converter with 12 bit

resolution. The range in X and Y is nominally selectable by software, allowing ¼, ½, ¾, or full range. "Full range" is selectable at the high voltage driver with a maximum capability of ±100 V. Typically the scanning voltages are symmetric about 0 V in both directions, that is, the center of the scan is (0 V, 0 V), but this can be offset both by software and at the high voltage driver. This slightly redundant arrangement is a result of the various previous methods of control. It may be desirable to remove the redundancy, although since the voltages recording the size of each scan are actual voltages recorded immediately before scanning this does not pose any difficulties in operation or in recording data.

THE FEEDBACK LOOP

Most important, of course, is control of the vertical position of the tip. We use an analog feedback loop, but digital feedback loops are becoming more common, especially with commercial STMs. The feedback loop consists of several stages: the current amplifier, the differential amplifier, the gain amplifier, and finally the high voltage amplifier, which sends voltages to the actuator. This loop is discussed in detail by both Firing and Cahill, but Cahill was concerned with tunneling current versus barrier height and employed a

logarithmic current amplifier for this purpose. The system is significantly different from what Firing used.

The first stage of the loop is the current amplifier or preamplifier. This amplifies the tunneling current from the tip. The preamp is an LH0052, used mainly because it draws a very low input bias current. This is

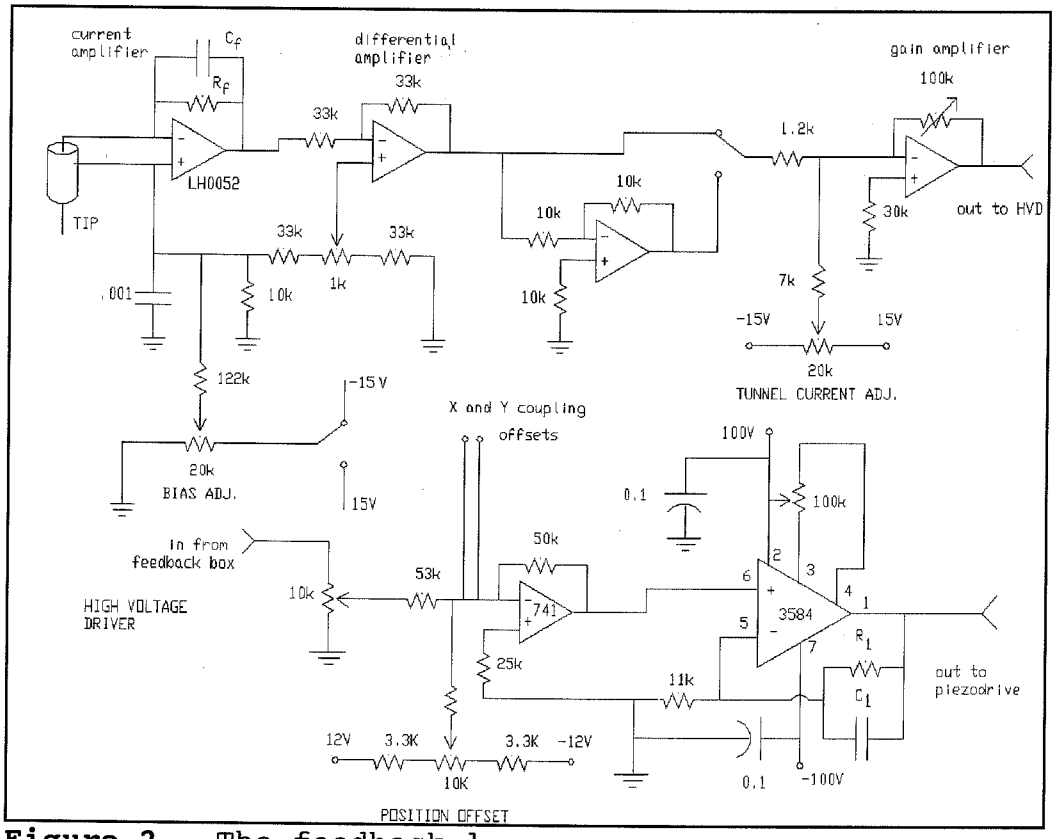

Figure 2 - The feedback loop

especially important since the tunneling current that we are measuring is also very small. It is located on the STM body in an electrically shielded box very close to the tip. This location reduces the susceptibility of the tunneling current to noise before it can be amplified.

The action of an op-amp can be easily understood by

considering that it will vary its output voltage however necessary to bring the voltage at the inverting input to same value as the non-inverting input. In the current amplifier the non-inverting (+) input of the preamp is connected to the bias voltage which is controlled by a external potentiometer. A 2000 MΩ feedback resistor, R_f, and a 10 pF capacitor, C_f, connect the output to the inverting (-) input. The inverting input is connected directly to the tip. The op-amp does not so much amplify a current, as its name would suggest, as translate the current into a voltage that can be used by the rest of the circuit. The best way to visualize how this occurs is by considering conservation of charge. When a current flows from the inverting input, i.e. from the tip, that current must be supplied by the output of the op-amp through the feedback resistor creating a potential across the resistor. This is the potential measured at the output.

This, however, is only for a constant current. As current varies with time the feedback impedance is also dependent upon the feedback capacitor. Assuming that a variation in current over a very short period of time can be represented by a sign wave of frequency ω, the voltage required at the output to supply this current to the input is:

$$V_t = I_o \frac{R}{1+i\omega R_f C_f} \quad \text{and its modulus} \quad |V_t| = I_o \frac{R}{\sqrt{1+\omega^2 R^2 C^2}} \; ; \; i=\sqrt{-1} \tag{1}$$

The parallel $R_f C_f$ combination also acts as a low pass filter[12]. The frequencies, f, that pass through this filter without significant distortion are:

$$0 \leq f \leq \frac{1}{2\pi RC} \tag{2}$$

This is an extremely important parameter in the operation of the microscope and we will return to it.

Since the non-inverting input is not held at ground, but at the tip biasing voltage, the output voltage of the preamp is not V_t, but a voltage which includes this bias voltage:

$$V_p = V_b + V_t \tag{3}$$

The undesired bias voltage is subtracted out by the differential amplifier. This is the next amplifier which processes the signal.

After the current from the tip has been amplified by the preamp it is much less susceptible to noise. A shielded cable runs from the STM to a rack mounted box where the differential amplifier and the rest of the low voltage portion of the feedback loop are mounted on a solderless breadboard. The bias voltage is run through a two-to-one voltage divider and fed into the non-inverting input of the op-amp. The resistor leading from the

preamp and the feedback resistor of the differential amplifier are the same providing another voltage divider for V_b. Let the current through the differential amplifier be I_d, the feedback resistor be R_d, the output voltage be V_d:

$$V_d - \frac{1}{2}V_b = I_d R_d = \frac{1}{2}V_b - V_p \quad \Rightarrow \quad -V_d = V_p - V_b \qquad (4)$$

The differential amplifier is an inverting amplifier.

The signal then may or may not go through the next amplifier of the circuit, which is a simple inverting amplifier with a gain of one. When the bias voltage is negative, the more common case, the invertor is bypassed. A switch can be thrown to switch the bias voltage to positive. When this happens the signal coming from the tip must be inverted, otherwise the tip would be drawn away from the surface when not in tunneling range and then, when it enters tunneling range, violently driven into the surface. The sign of the bias voltage and the output of the invertor are connected to the same double pole, double throw, two position switch so that they cannot be inadvertently mismatched.

The next important element of the circuit is the potentiometer that controls the tunneling current about which the feedback loop operates. When a tunneling current is present the preamp outputs a certain voltage which corresponds to that current. This voltage is

wholly dependent upon R_f (assuming only low frequency changes in tunneling current) and is simply equal to $-I_tR_f$. The output of the differential amplifier and the gain amplifier is zero in the absence of a tunneling current. Ideally we want it to be zero when some optimal tunneling current, I_o, is present. A current is chosen - typically on the order of 1 pA - and the "Tunneling Current Adjust" is set at:

$$V_t=I_oR_f \qquad (5)$$

V_t is opposite in polarity to the response of the loop to a tunneling current. When the tunneling current is I_o, V_t is exactly offset by V_d (equ. 4) and the output signal is 0 V.

Before the signal is sent out to the high voltage driver it goes through one more op-amp. This inverting amplifier has a variable gain by means of the variable feedback resistor. This allows a grater range of loop gains and is usually set so that the output of the gain amplifier has some whole number value relative to the tunneling current, e.g. 1 nA/V.

The final step in the loop is the high voltage driver. First the signal is run through a variable input so that the gain can be easily controlled. This is where the effective range of the feedback mechanism is decided. A 10 kΩ, 10 turn precision potentiometer acts as a voltage divider to determine the level of the signal

input to the high voltage op-amp. The input gain has been calibrated experimentally to determine the dependence of the vertical motion of the tip on the gain setting at this point. With the present configuration this value is 1 nm V^{-1} γ_s^{-1}, where γ_s represents the value shown on the dial of the input gain control, $0 \leq \gamma_s \leq 10$, and V represents the voltage of the feedback loop directly following the differential amplifier.

The high voltage driver operates exactly as the rest of the loop. It consists of two op-amps, one acts as a buffer and inverts the input signal. The second is a non-inverting amplifier with a gain of 10 and is capable of outputting ±100 V.

What is actually important in the feedback loop is the behavior of the loop as a whole. This is what determines the resonant frequency of the loop and the bandwidth of the loop. These parameters are calculated in detail in Firing[13]. I will simply restate his results here.

Defining:

V_o = high voltage driver offset voltage
Γ = $\gamma_p \gamma_h \gamma_t \gamma_a$
ν = frequency of the signal on the loop
δ = separation of tip and surface
γ_x = the gain of an amplifier x
ω_x = the bandwidth of amplifier x,

Subscripts:

p = low voltage portion of the feedback loop

h = the high voltage amplifier

t = the tunneling phenomena itself

a = the piezoelectric actuator

the signal around the loop can be written:

$$\xi = \frac{V_o\Gamma + \delta\gamma_p\gamma_t(1+i\frac{\nu}{\omega_h})}{(1+i\frac{\nu}{\omega_h})(1+i\frac{\nu}{\omega_p})-\Gamma} \qquad (6)$$

The value of Γ cannot be determined precisely since the gain of the tunneling effect, γ_t, varies greatly with δ. It is assumed that the bandwidth of the piezoelectric is very high, and the bandwidth of the tunneling effect is considered infinite[14].

The resonant frequency of the circuit can be calculated by setting the denominator equal to 0:

$$0=\nu^2-i\nu(\omega_h+\omega_p)-\omega_h\omega_p(1+\Gamma)$$

$$\omega_{res}=i\frac{\omega_h+\omega_p}{2}\pm\sqrt{-\frac{1}{4}(\omega_h+\omega_p)^2+\omega_h\omega_p(1+\Gamma)} \qquad (8)$$

Due to the high frequency oscillations mentioned earlier, the bandpass frequency of the current amplifier was significantly reduced by increasing C_f. Now ω_h and ω_p differ by only a factor of four. While this violates the theoretical calculations by Firing suggesting that the bandwidth of the current amplifier remain at least an entire order of magnitude different from the bandwidth of

the high voltage driver, it was successful in raising the gain achievable significantly. The theoretical problem being that when the bandwidths are of the same order of magnitude the Q factor, or quality factor, of the loop increases significantly. This would allow noise at the resonant frequency of the loop to resonate causing an oscillation. The noise level of the circuit was low enough to avoid this problem and the low pass filter at the current amplifier was helpful in reducing the tip oscillations.

One modification to the feedback loop that proved useful was to divide the Z output of the high voltage driver by 10. This was done to reduce the noise from the high voltage op-amp. There was a significant improvement in the gains attainable (calculated with the voltage divider taken into consideration) without oscillations. This also reduced the overall range of the actuator by a factor of 10 to a total range of 250 nm. While this is not a problem with very flat surfaces such as gold, it could be prohibitive in scanning rougher surfaces.

Another difficulty with the reduced range is bringing the tip into tunneling range with the surface. The vibrations created by turning the micrometer on the STM can easily swamp the feedback loop, crashing the tip into the surface. In order to solve these difficulties a switch was wired into the high voltage driver to allow

easy access to both the full range of the piezoelectric, for bringing the sample into range, and to the reduced range, for scanning. Using a three position, double throw, five pole switch, the ability to divide the X and Y voltages independently of the Z range was added.

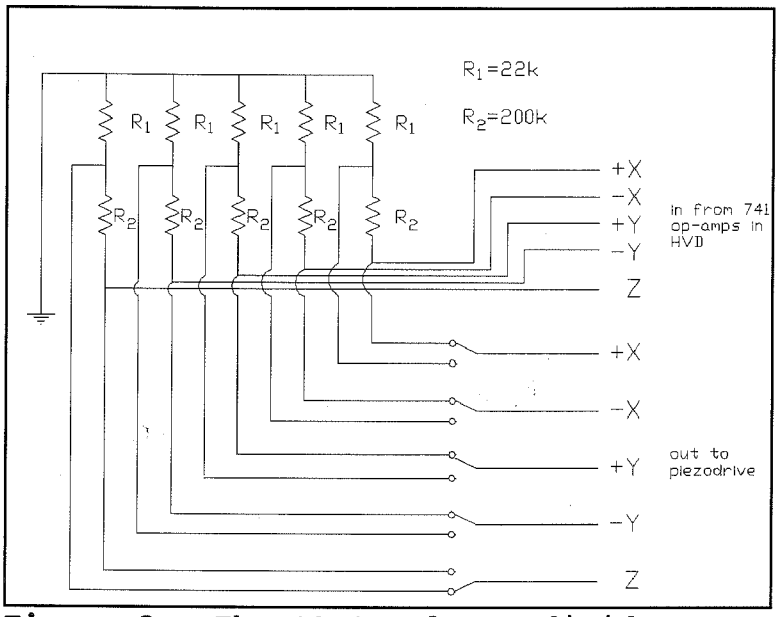

Figure 3 - The 10:1 voltage divider switch

As was mentioned previously, the tip oscillations are highly dependent upon the loop gain, and this reduces the exploitable vertical range. Because of the short range available, the coupling between the vertical and lateral positioning of the tip became prohibitive to good scanning. Over any sizeable lateral distance the tip would quickly move out of tunneling range. To remedy this a corrective offset was added into the Z signal. This is done simply by adding a fraction of the signal from the X and Y channels into the Z loop. The configuration is shown in Figure 4.

The manner in which scans are conducted is that the

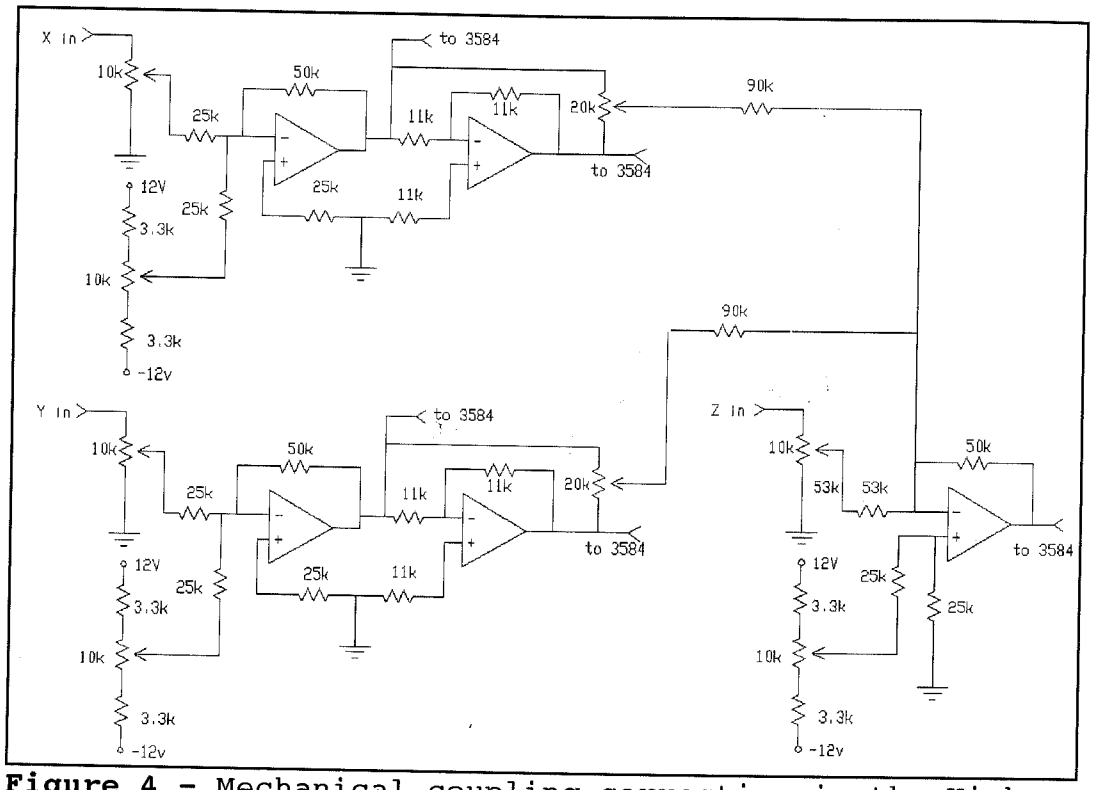

Figure 4 - Mechanical coupling correction in the High Voltage Driver

tip is stepped slowly along the line while data are recorded, at the end of the line the increment is stepped and the line resets *immediately*. This violent return occurs as fast as the actuator can respond to the voltage change (slew rates of the op-amps are considered infinite). There is no reason that the tip should not crash into the surface as this occurs and large spikes in the feedback signal during this return indicate that this may be happening. The computer is programmed to delay each line several hundred ms after the return to insure that these spikes are not recorded with the data.

A solution to this problem was designed and implemented. A signal was sent to one of the digital out

bit connections of the DT2801 at the end of each scan line. The signal was added into the loop through a buffer to lift the tip out of tunneling range and out of range of the highest point on the surface. Once the tip had returned to the beginning of the line it was dropped back to tunneling range again.

It is believed that this process was successful in avoiding the surface during the line return. But, possibly due to the large displacement it caused in the Z motion, it would take the tip nearly thirty seconds to resume its previous position after the lift was executed. It returned to tunneling range and asymptotically drifted back to its stable position. For this reason the lift was bypassed. The software and buffer are still in place to accommodate this, it may be attempted again with a more limited displacement to reduce this side effect.

THE COMPUTER

Finally, the actual controlling of the scan is done by a modest 8088 processor PC. A Data Translations DT2801 DA/AD converter interfaces the computer with the control electronics of the STM. The DT2801 has two 12 bit DACs which are used to run the X and Y channels. These voltages from the board are sent directly to the high voltage driver. The signal from the feedback loop is taken immediately before the input of the high voltage driver. It is sent to one of the 12 bit ADCs and

recorded as a 12 bit integer. The DT2801 is a monster created before people had crazy ideas like "user friendly." The first trip through the "User's Manual" is unnerving at best, but the board is ultimately functional with some powerful features. Anyone planning to program the STM must be intimately familiar with the DT2801 in order to program effectively. A considerable amount of time was put into programming the computer to run scans and record data. A truly thorough explanation of programming to run the scans, take the data, and then to process and display the data would be a monumental task worthy of an Honors Thesis in its own right. I will summarize what has been done and make suggestions for any future programming attempts.

There is only one program now in existence to run the STM. The bulk of the routines were written by Bill Cahill, although he never actually had the opportunity to run the program. His language of choice was C++ and for this reason (much to the dismay of Fred "QBASIC" Ellis) all related programming is also in C++. The control program by Cahill was modified to add a significant amount of software control over the scan was added.

The data that are stored are actually one dimensional. The parameters (ranges, number of lines, data points per line, etc.) of the scan are stored with the data and the lateral position of each point is

recreated when the file is retrieved. Since the data written to the file are the 12 bit integers output by the ADC, the data are stored in a compacted form to save space in the normal 8 bit byte file format. Any attempts to analyze the data must take into account the format of the data files as created by this program. Anyone planning on programming for the STM should refer to Appendix A in Cahill and should review the current software thoroughly.

I have also written a functional program for displaying the scans. Although the program does a more than adequate job of displaying the data on a VGA monitor in a "3-D" image, it has only a limited ability to analyze the data. This analysis will be discussed in Part II, so I will not go further with it here.

It has been suggested that we use a commercial program designed for analysis of data of this type. This approach has not been used so far due to a personal attachment to the program which reads the scans and due to programming difficulties that would be involved. The format used to record the scans would have to be altered to create data files compatible with the program in use. While this is not a problem in programming, reality can pose difficulties. The Leading Edge PC and the DT2801 are not necessarily the best instruments for handling large quantities of data. Their capabilities could

easily become the limiting factor in how fast scans can be taken. One solution to this problem would be an intermediary program to expand the compacted files to a usable format. Such a program could easily be made to convert the files into any number of formats.

With the peculiarities of the STM and of the DT2801 I, strongly recommend using the program already developed for running the STM. The routines written by Cahill for scanning and recording are very efficient and the user interface has been improved to allow more than adequate software control of the STM. If the STM is automated further, routines can be easily added for that control as well.

As far as data analysis is concerned, it is time to move up to the big leagues. Many programs are available on various computer networks. Appropriate software should definitely be investigated. The STM is already capable of taking reliable data and its resolution will certainly improve. It will be ultimately much more efficient and produce better results to invest some time in acquiring and implementing professional display and analysis software.

CHAPTER III: OPERATING THE STM

This is the truly "hands on" portion of the thesis. Those interested in the characterization of gold should skip right to the pictures. I will give a detailed description of the do's and don't's of running the STM.

My first suggestion is not to pull on the inside doorknob on the door to room 50 facing the stairwell. It is broken and will come off in your hand.

TUNING UP

The first task is to properly set the multitude of gains and offsets in the feedback loop. Although the operator is faced with a senseless array of amplifiers, voltage dividers, and RC filters, no electronics knowledge beyond Ohms Law is really needed. Well, almost none.

The first parameters to be chosen are the tunneling current and the bias voltage. All scans in this thesis were done with a tip bias voltage, V_b, of -100 mV, and a tunneling current, I_o, of 0.5 nA (type.) A resistor is chosen of the value $R_t=V_b/I_t$ and placed between ground and the input to the current amplifier. This is not necessary, but is done to insure that the loop is working

properly. The bias voltage is measured directly from a standard bnc plug on the box housing the low voltage feedback components and is adjustable by a pot on the same unit.

With this resistor in place the output of the low voltage variable gain amplifier is monitored. The "Tunneling Current Adjust" is fixed to offset the voltage of the tunneling current. That is, it is varied until the output of the amplifier is zero. In this manner the output of the circuitry is adjusted so that when the tunneling current is precisely at the predetermined value, I_t, the output will be zero volts. The feedback loop and the piezodrive are then able to respond in both positive and negative directions.

It is often the case that a resistor of the value R_t as calculated above is not available. In this case the calibration can be done, but is slightly more involved. First, the offsets of the loop should be set to zero. If the signal is being read from before the adjustable gain amplifier, then only the Tunnel Current Adjust must be set to zero. If the voltage is to be read from the output of the HVD, which can be convenient, the offset of the HVD must be zeroed and the gain set to a known value, γ_h. At this point the feedback loop is open (we're doing this because we didn't have the right size resistor to close it) so at any point after the differential

amplifier the loop is at 0 V.

The gain from the tunneling current to the output of the HVD is:

$$\Gamma = \gamma_i \gamma_g \gamma_h \gamma_{adj} \; ; \; \gamma_i = \frac{V_f}{I_t} \qquad (9)$$

If the feedback loop is to be at 0 V at a chosen tunneling current, I_o, then we want to set the Tunnel Current Adjust so that when the loop is open there is an observed voltage of $-V_o = \Gamma I_o$ (when observed at the input of the gain amplifier $V_o = -\gamma_i I_o$). With this offset in place you can convince yourself that when the loop is closed and there is a tunneling current of I_o that the observed voltage at either point in the loop will be 0 V. Currently R_f=2000 MΩ, the output of the current amplifier must be at 2 V (actually 2 V + V_b) to follow a 1 nA current, so that the gain of the current amplifier γ_i= 2 V/nA. The bias voltage is taken care of by the differential amplifier, which has a gain of 1.

γ_g is the gain of the adjustable gain amplifier. This is usually set so that the voltage being measured after it has some convenient whole number value in terms of nm/V. It is even more useful to speak of the value as a function of the gain setting on the HVD. In this manner the signal is considered to have meaning in terms of nm/V/γ_h. This value was experimentally determined by a calibration of the Z response of the crosspiece and is

approximately 15 nm/V/γ_h, where the gain value is a number from one to ten representing the number of turns of the gain pot.

This process only needs to be repeated when you want to change some parameter of the loop.

FOCUSING

The sample is placed in the holder and has been brought close to the tip under the optical microscope. It is best to bring the tip as close as possible before starting with the fine micrometer under feedback conditions, otherwise the "focusing" process can be extremely tedious. The feedback plug and the high voltage plug are now connected.

The vibrations that occur when the micrometers are being turned are more than enough to crash the tip, so extreme caution must be taken at this point. The toggle switch controlling the 10:1 voltage dividers should be set in the "FULL Z" position. In this mode the full ±100 V of the HVD are available (to the offset, not to the feedback mechanism). This is a range of nearly 3000 nm. Four full rotations of the fine adjust micrometer produce approximately the same motion. The gain setting should be at least 1 on the 10 turn pot scale.

As the signal leaves the feedback control box it is

sent simultaneously to the HVD, the computer, and to an oscilloscope. The HVD offset is used to bring the tip as far toward the surface as possible while at the same time watching the oscilloscope. When the voltage on the oscilloscope drops the tip is tunneling. When the maximum Z offset has been reached and no tunneling occurs the offset is backed off completely and the mechanical fine adjust advanced two revolutions. The HVD offset is again used to bring the tip towards the surface. The procedure is repeated until the surface is found.

The fine adjust is sensitive enough so that the tip can be positioned with the HVD offset at or near zero when in tunneling range. The tip must be backed out of range of the feedback loop before any mechanical adjustment is made. Once the HV offset is zeroed the STM is allowed to sit in its enclosed box for at least an hour, and often overnight, with the tip backed far out of range. This allows time for the STM to reach thermal equilibrium. The time at which the drift has sufficiently subsided is determined by observing the stability of the feedback signal on the oscilloscope with the tip held stationary while tunneling. Once the thermal drift has subsided the HV offset is again zeroed and scanning begins once the vibrations have been damped out. 20 minutes is usually adequate.

In chapter I, I discussed the mechanical coupling

between vertical and horizontal motions of the crosspiece. Here is where the adjustment must be made. There are two potentiometers inside the HVD marked X and Y. They determine the portion of the X and Y signal added to the Z signal for compensation. This adjustment is complicated by the 10:1 voltage divider.

The corrective offset was designed before the voltage divider was considered, thus corrections are made before the high voltage amplification. The voltage divider is after the high voltage amplification and does not necessarily divide all three directions, normally it only divides Z. The STM is now calibrated to run most efficiently in this mode, so the correction must be adjusted in this mode.

To make the adjustment the tip is brought into tunneling range with as high a gain as is stable. The offset of one of the lateral directions is manually swept from one end of the voltage range to the other while watching the feedback signal on the oscilloscope. Surface features keep the signal from responding directly to the lateral position, but a general slope can be determined. The internal pot is adjusted and the lateral range swept again. This is done in both X and Y. Remember that the coupling in the Y direction is non-linear so I did the calibration for deviations not far from zero. A much smaller correction is necessary in Y

than in X.

SOFTWARE SELECTIONS

The scanning software is menu driven. "Line" refers to the coordinate being rapidly stepped; "increment" refers to the direction stepped after each "line" has been scanned.

The length of the line and its offset are both adjustable in increments of ¼ of full range. The number of data points per line is independently chosen to be 256, 512, or 1024. The number of lines can be any integral value from 1-4095, but since the DAC only handles integers, values are usually chosen to be powers of two. No error will occur from other values, but scan lines will not be evenly spaced and this will not be reflected when the data is retrieved. The length of the scan and the offset are also continuously adjustable.

The rate at which data is taken must also be selected. For the optimum rate the bandwidth of the feedback loop must be known. If the limiting bandwidth of the loop is $f=(1/2\pi RC)$, then the rate of taking data should be $2f$. This is the maximum rate at which the loop can respond to a changing tunneling current with acceptable distortion. Data taken at a faster rate will be redundant, measuring only the response of the loop, no

new information can be gained. Since the line is digitally stepped according to the number of data points being taken, no information is lost in scanning more slowly, but the scan rate should be as high as possible to reduce effects of noise and thermal drift.

The actual mechanism for controlling the scan rate is the on board clock of the DT2801. From the user selected line frequency a setting for the clock is calculated and implemented. The board is capable of a sampling frequency of 300 Hz with the present software. This may ultimately be a limiting factor, but is now a factor of 20 higher than what the feedback bandwidth will permit.

Here the emphasis on increasing the bandwidth of the feedback loop becomes apparent. With the 8 Hz bandwidth of the current amplifier a very modest scan resolution of 64 lines, 256 points per line, takes 18 minutes. A respectable scan of 128 lines, 512 points per line takes over an hour. By comparison, Emch *et al.*[15] report a line rate of 80 Hz, taking a 1000 line scan in 12 seconds. Putnam *et al.*[16] report scan rates ranging from 25 Å/s to 500 nm/s.

Either X or Y can be used as the line direction by simply switching the coaxial cables coming from the DT2801 box. When this is done the connections from the HVD display to the DT2801 must also be switched in order

for the scale of the scan to be properly recorded. The X and Y responses of the actuator are different[17], so the scaling of the data when read must be changed accordingly. This is provided for neither in the information data structure of each data file nor the program used to read and analyze data. The orientation was recorded in a lab book and images scaled accordingly.

Of course all of the details and idiosyncrasies of the STM cannot be given here. There are many calibrations to make on the STM before it can image effectively, but once they are made it becomes possible to image surface topography, which facilitates further improvements of the STM by evaluating its performance as well as providing valuable data.

PART II:

A PRELIMINARY INVESTIGATION OF GOLD DEPOSITED ON GLASS

INTRODUCTION

Since the beginning of the development of this STM, the goal has been to eventually use the instrument to characterize the surface topography of evaporated thin gold film. Up until this point the research has focused mainly on development and performance of the instrument itself. While Part I of this thesis demonstrates that the development is not complete, the STM has already provided us with the first data on this topography. The findings of this thesis are extremely encouraging in that they essentially prove that the novel piezoelectric actuator, the body construction, the electronics and the environment of the STM are fully capable of achieving the goal of the project. Furthermore, after review of the available literature on Au surfaces the STM should be able to provide sufficient data for publication of a study of evaporated gold films deposited on glass.

CHAPTER I: BASIS FOR INVESTIGATION

Here the existing body of literature on the topography of gold surfaces is reviewed. Previous work is cited for comparison and the need for further work in this area is demonstrated. The experiments are also described.

REPORTED KNOWLEDGE

The existing body of published research on the topography of gold films are focused mainly on finding a suitable substrate for STM studies of other materials such as biological molecules[18,19]. This work deals largely with gold deposited on cleaved mica surfaces. The articles portray various, if not contradictory, characteristics of gold topography on mica. They also indicate that the deposition conditions such as the method of deposition, temperature of the substrate, and vacuum conditions play a major role in the growth of these films.

After extensive research I have only come across two published STM images of gold evaporated onto a glass substrate. One of them was of a sample deposited at over 700 K.[20] Our samples were deposited at room temperature with only slight warming due to radiative heating. The

contrast of features of gold on mica deposited at such disparate temperatures gives reason to believe our surface should bear little resemblance to this image, and indeed it does not.

The other image, reported by Schneir et al.[21] is of gold evaporated in conditions very similar to ours, but using a 7 Å layer of chromium as an adhesive on the glass substrate and a slightly higher deposition rate. This image shows very similar features to what we have observed. In both cases the topography of gold on glass were not the object of study, but only presented in contrast to another surface, gold on mica in the first case and gold facets in the second.

This literature can give us some idea of what kind of characteristic features we might find, but there is no way we can use these studies to confirm or dismiss what we find. Emch et al. [22] report atomically flat terraces of hundred of angstroms with abrupt ridges of high densities of atomic steps. They also attribute previous images of "rolling hills" (precisely what we saw) on gold surfaces to contamination of the tip or a blunt tip. Their images are impressive and convincing. This would seem to void the findings of this thesis, but our images are on glass at much lower temperature. Also, our images are qualitatively different from theirs and could not have resulted from low lateral resolution imaging of a

similar structure. Their data are also passed through a high pass filter before being recorded, then through a digital low pass filter before being sent to a graphics work station where it is processed into a continuous grey scale image. This may eliminate the low contrast features (read rolling hills) that we observe.

Though a number of STM studies of surface topography of gold films have been published, there is clearly need for a characterization of evaporated films on glass slides. These surfaces are of interest not only to Professor Ellis for modeling the substrates of his superfluid ^{4}He third sound work, but to a great number of researchers using gold on glass substrates for various purposes. Gold on glass offers a much larger surface area than facets and is much easier to prepare than gold on mica.

THE EXPERIMENTS

The microscope was run exactly as described in Part I. The tip bias voltage was -100 mV and tunneling current typically .5 nA for all scans. All scans were taken in air. Typical scan rates were 15 data points per second (17/34 seconds per line for 256/512 points per line) with little variation on this rate.

The Z response was calibrated by first calibrating

the fine adjust against the coarse adjust and then the actuator motion against the fine adjust. X and Y were calibrated by placing a sample at 45° to normal and measuring Z response as a function of X and Y. The lateral calibration is ±20%. This high margin is due to the irregularities in the surface and the extreme instability of the tip at such an angle to the surface. The calibration should ideally be done by measuring a crystal lattice constant (for X and Y) or a known atomic step (Z). This is a standard method of calibration.

PREPARATION OF THE SURFACE

Virtually every report cited in this thesis agrees that gold films on any substrate are highly dependent upon deposition conditions, with temperature of the substrate having the most noticeable effect. For our samples, 99.9% gold pellets were evaporated from a tungsten basket which was resistively heated. Impurities were burned out of the gold before the substrate was exposed to the evaporation. The target was a standard borosilicate glass microscope slide located ≈15 cm directly above the evaporation basket with an angle of incidence of the evaporated particles of 90°. Pressure in the vacuum chamber was on the order of 10^{-7} Torr. Thickness of the films was approximately 1000 Å as

determined by a quartz crystal oscillator monitor. Deposition rate was typically 1.5 Å/s.

No measures were taken to control the temperature of the substrate during evaporation. A rough measurement of the effect of radiative heating showed that the substrate temperature increases almost linearly for eight minutes and then begins to level off asymptotically as the substrate reaches equilibrium. Starting at room temperature, 273 K, after ten minutes (typical duration of evaporation) the temperature was 350 K and would likely increase only slightly with further exposure.

Scans were taken of surfaces exposed to air for months and some exposed for only a few hours. No dependence on age of the sample or tip was found in image quality or surface characteristics. It should be noted however, that these data are the first obtained with this microscope. While they can be used to determine surface characteristics, more than anything they merely demonstrate the functionality of the STM. Conclusive characterization of gold surfaces will require an investigation concentrating much more on the surfaces themselves rather than on the operation and performance of the STM. All images presented are data as recorded with no filtering outside that of the feedback loop and no other processing of the data.

CHAPTER II: DATA AND ANALYSIS

In this chapter the data gathered with the STM are presented. The performance of the STM and the validity of the data are discussed. Finally, a model for the of evaporated gold films on glass is presented and the parameters of the model quantitatively determined.

THE DATA

Figures 5 and 6 demonstrate most clearly the ability if the microscope to provide reliable data. They are taken in immediate succession at the same location with a slight change due to thermal drift. The images are very similar, but it is apparent that they are not identical. Most reports attribute such changes to surface self-diffusion[23,24,25,26] of gold. The experimental nature of the STM at this point does not allow me to make such a conclusion. However, given the long duration of our scans this is certainly possible. Another reason could be slight changes in the tip or surface produced by the "return trip" of the tip as discussed in Chapter II, Part I.

In both cases the scan direction is right to left for the line and front to back for the increment. The scales refer to the entire length and width of the scan

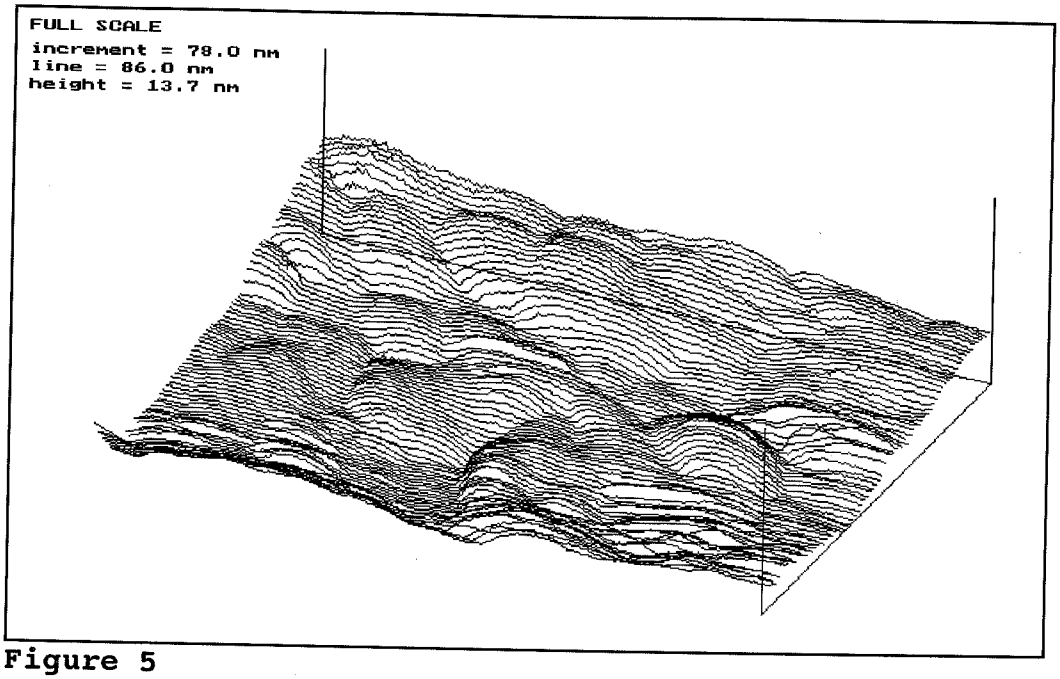

Figure 5

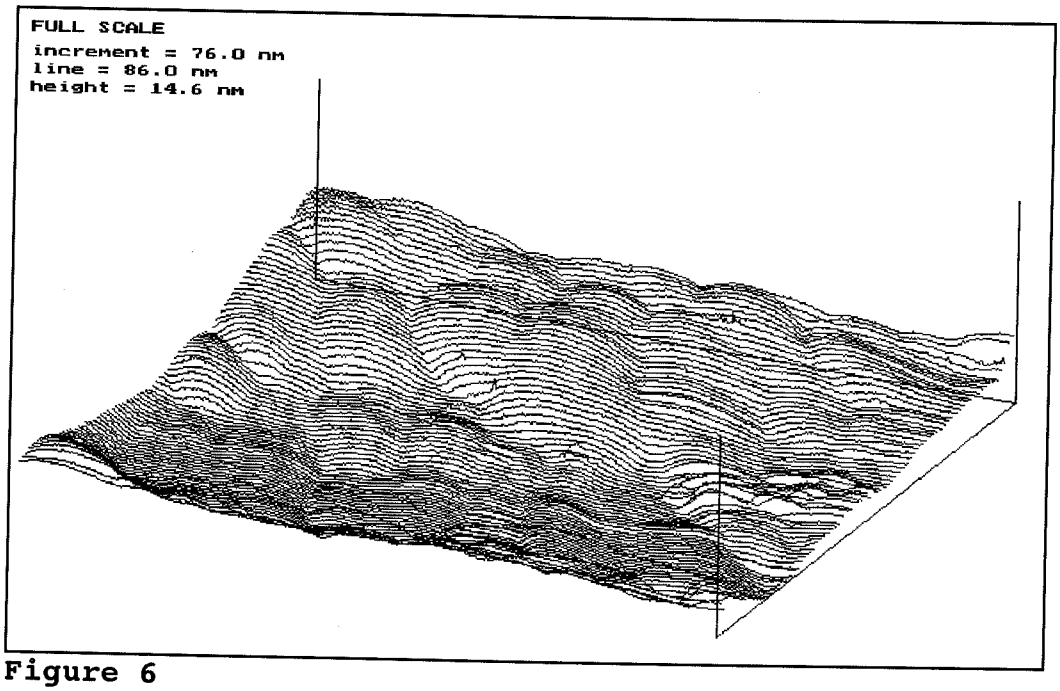

Figure 6

for "line" and "increment," but the "height" scale refers to the length of the vertical bars at the corners of the image, not to the highest and lowest points of the image.

These surface features compare well in size and shape to that reported by Schneir et al. Their gold film was similar in preparation except for a 0.7 nm chromium layer deposited on the glass to improve adhesion to the substrate and a slightly higher deposition rate. The thrust of the paper was facets on balls made by melting gold wire in an acetylene flame.

It is commonly acknowledged that STM images are influenced by the geometry of the scanning tip. This is often dependent upon both scan direction and scan rate[27] and can manifest itself simply as low resolution and also as a "double tip" where some features of the of the surface are imaged multiple times[28]. There is no way to tell from a single image what data are meaningful and what are not. Even identical scans do not eliminate the possibility that they were both influenced by tip geometry. In fact, it is more likely that they will just be identical convolutions of the tip and surface.

One way to verify this is to scan the tip in different directions across the same location. Figure 7 and 8 represent an extreme case where tip geometry has altered the image.

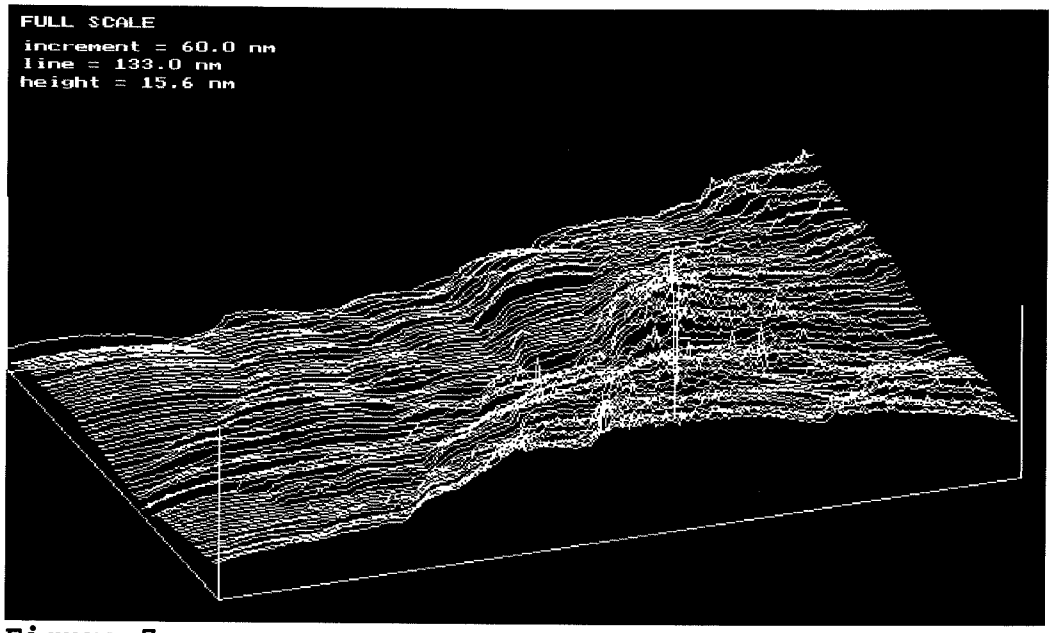

Figure 7

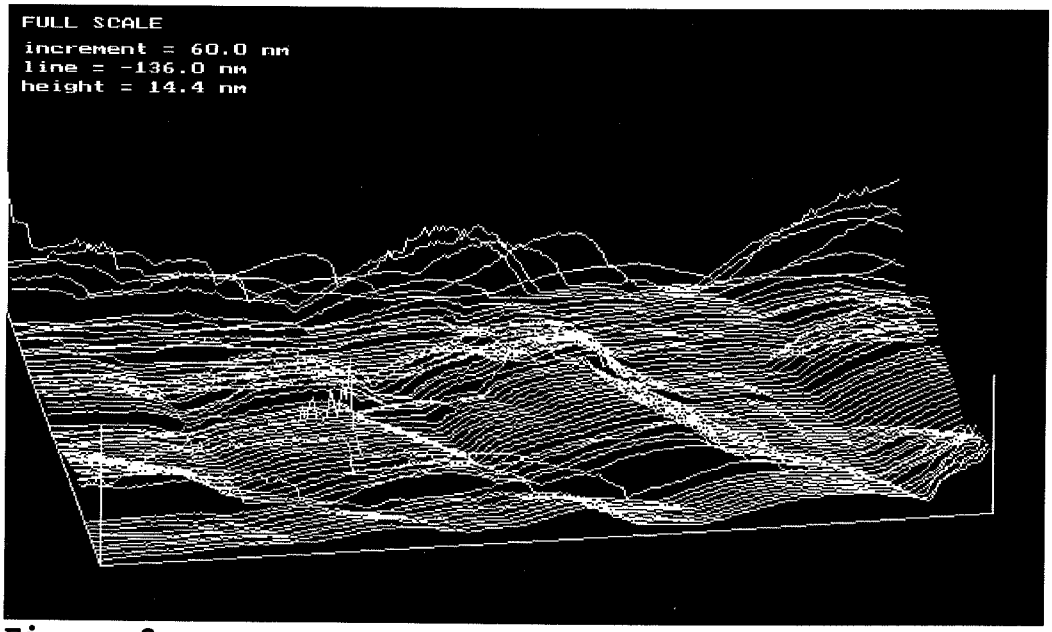

Figure 8

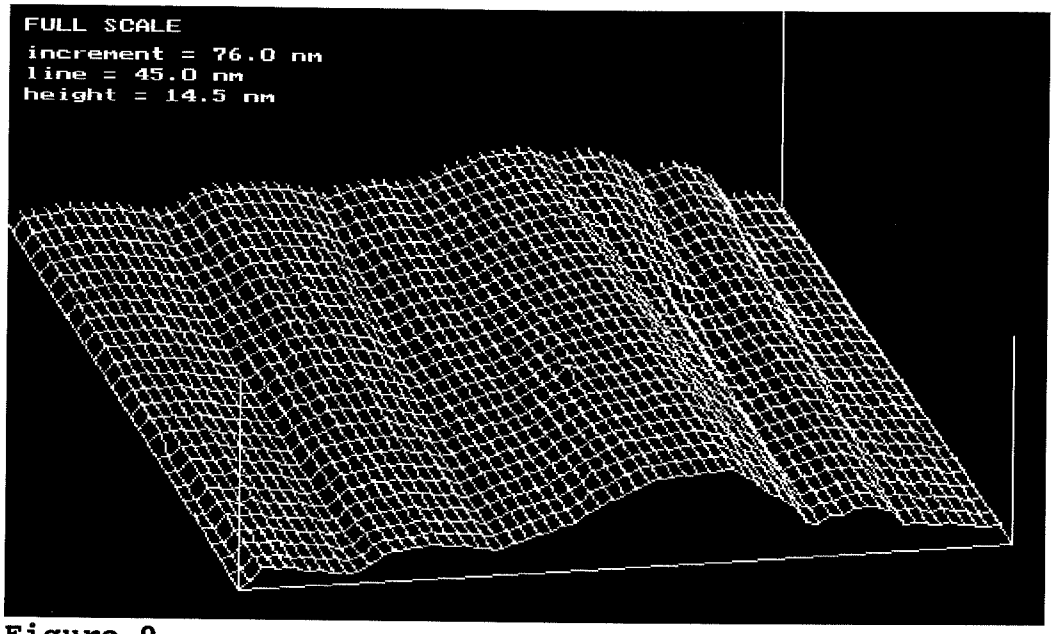

Figure 9

In the two scans the direction in which the line was scanned was reversed by running the control signal through an invertor before sending it to the HVD. The voltage range was symmetric about zero so that the inversion did not change the location. Even though both images are quite noisy it is apparent that they are dissimilar. They should be mirror images of each other with the mirror located either at the right end of 7 or the left end of 8. The increment direction is back to front for both and the location was not changed.

If the image is similar when scanned in different directions it is likely that the reproduction is true to the resolution where the symmetry in the images ceases. Figure 9 and 10 are images of the same location. In 9 the line direction is X, from the reader into the page.

The grid pattern is not created by two scan directions, but by lines added perpendicular to the scan lines to help visualize the contours of the surface, they do not represent data. For 10 the Y direction is used as line,

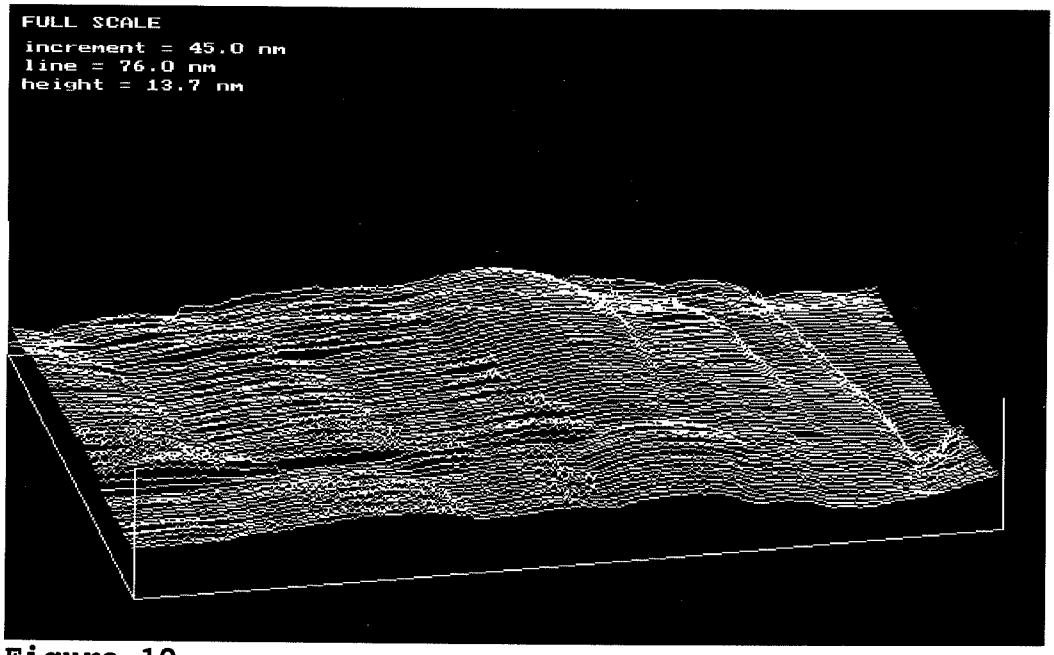

Figure 10

and X as increment. The way the images are rotated here they are reflections of one another. Front and back are reversed but left and right are equivalent.

The ideal characterization of a surface would be one basic, easily described feature repeated many times at regular intervals, as in a crystal structure. Another convenient model might be congruent features of different sizes randomly distributed composing the surface. The previously reported image by Schneir et al.[29] and many of our images confirm such a model with a spherical dome as a basis. The images are typically isotropic.

Figure 11 provides a more detailed image of a location different from that in Figure 5, but showing similar characteristics. Figure 12 is included to demonstrate even more clearly than Figure 5 the

Figure 11

reproducibility possible with the STM.

Not all scans show such features. Figure 13 is a clear example of what appears to be two rather flat regions separated by two abrupt steps of 3-4 nm height each. For comparison, assuming an fcc (111) orientation of the surface plane, one monolayer step is expected to be 2.4 Å[30].

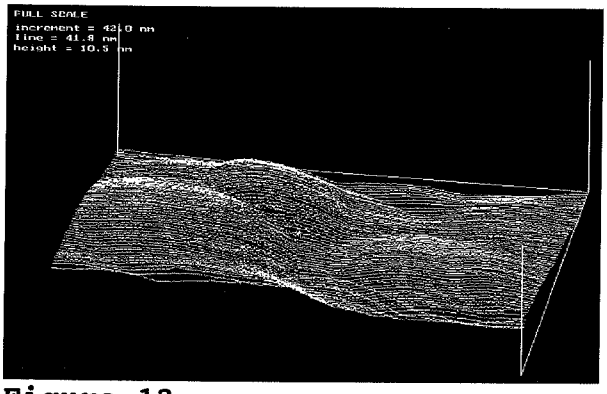

Figure 12

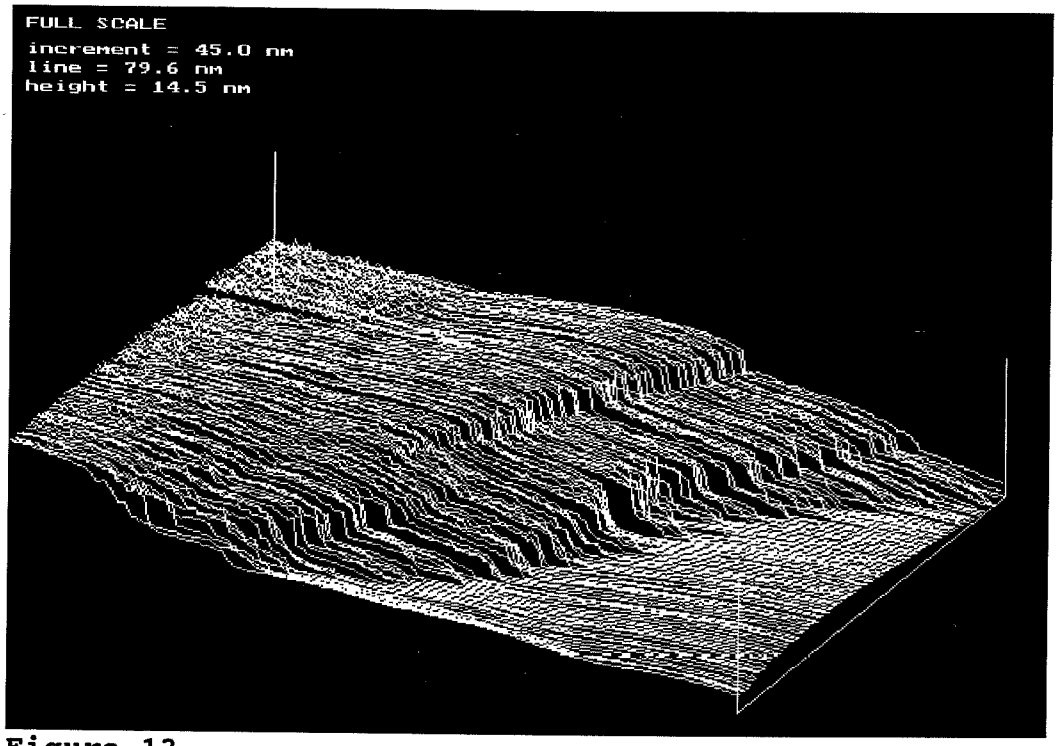

Figure 13

It can also be distinguished that the steps are not uniform edges but irregular ragged edges. It is unclear why this is the case, but this characteristic appeared repeatedly. Also, given the relative infrequency of such steps it can be assumed that they generally recur on length scales much greater than several hundred nm. Higher resolution of the STM will be needed before determining exactly how flat such regions are and a wider range will be necessary to determine the spacial frequency with which such steps occur.

Figures 14 and 15 show other types of surface topography observed.

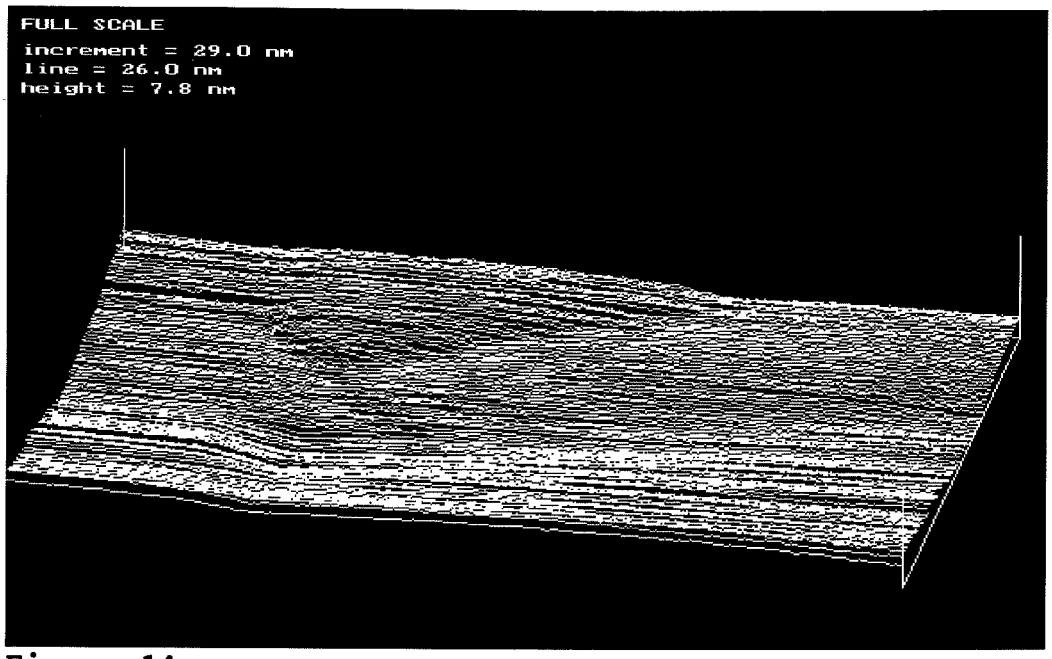

Figure 14

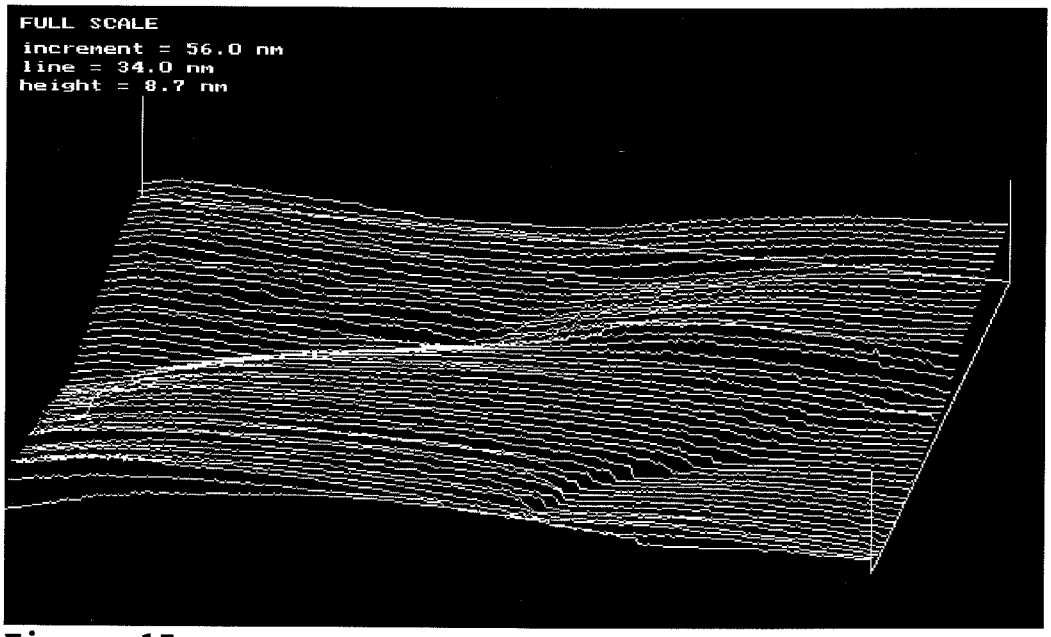

Figure 15

ANALYSIS

In order to quantitatively describe the surface a model for the surface must be adopted and a means of evaluating the parameters of that model must be found. From the images we have collected an appropriate model is a slightly more concrete version of the "rolling hills" description found in the literature.

From the data collected it is apparent that these hills are smooth except for where they meet. The junction of two smooth hills is a sharp angle. The hills are thought of as spherical sections which are truncated once they meet another spherical section. I will refer to these sections as *domes*.

There is evidence both supporting and refuting the notion that this is actually the topography of the surface. If one considers the interaction of the geometry of the tip and the geometry of the surface we find an immediate problem. The tip must have some finite radius of curvature limiting the resolution. Figure 16 shows just one way that the domes that we have observed could result from a blunt tip.

There are various reasons to believe that this is not the case. First, the domes were observed even when another image displaying different features had been taken with the same tip. Also, what we observed is very

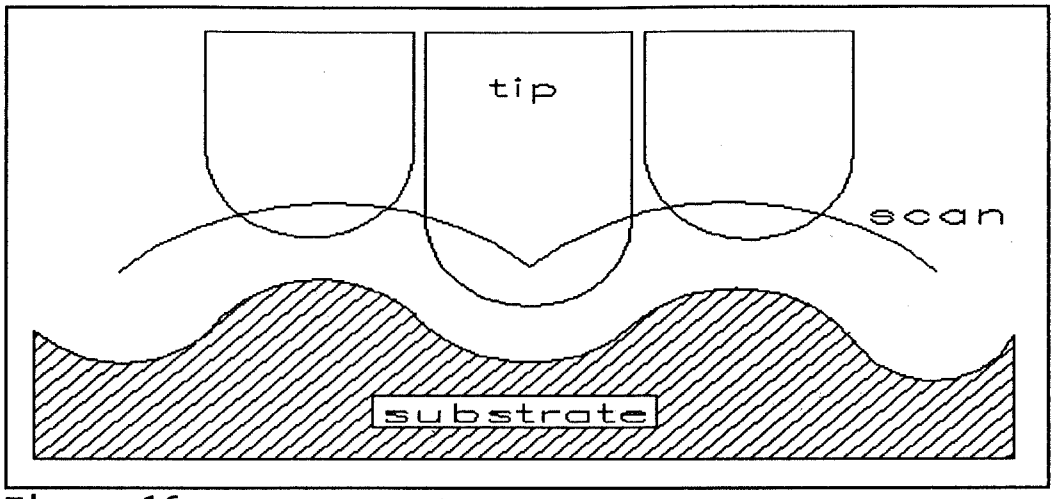

Figure 16

similar to the reported images by Schneir *et al*. Other images they presented of gold facets regularly resolve features much smaller than these domes. Perhaps the most convincing argument is that these features would support the theory of islet formation during evaporated film growth. In this process the atoms of the evaporated metal do not distribute themselves as isolated atoms on the substrate, but form islands on the surface. Such islands were observed by Binnig and Rohrer[31] in a gold film on silicon that had not yet reached the thickness required for a continuous film.

A continuous film is expected at a thickness of about 50 nm. Although our film are twice as thick as this, it is still very likely that the surface closely resembles the surface immediately after the film formed. Actually, most accounts agree that film thickness has little effect on the topography of the surface. This is

especially true at lower deposition temperatures (around room temperature) and is attributed to the low mobility of gold atoms on a gold surface at this temperature[32]. In this way once the gold has formed a complete layer at low deposition temperatures the surface should vary little with thickness.

Within this dome model it should be possible to get a full, although generalized, description of the surface in terms of three parameters: the radius of curvature of the domes, r_c, the height of the dome h_c and the distribution of these parameters about the average, σ.

In order to get a truly accurate measurement of these parameters data should be analyzed in all directions. If our data were isotropic, e.g. 256 points per line with 256 lines of resolution, this may have been possible by treating the data as a three dimensional array of values regardless of scan direction. This approach has its problems, however. Remember that the surface features are scan direction dependent. While we try to minimize this effect in the data that we consider valid, there is certainly some influence of the line direction in the data. There is also the problem that considerable time elapses between the recording of adjacent points in the increment direction. This allows low frequency noise to have a greater effect on the statistical variation of these adjacent points.

Bonnell and Mitchell[33] present these arguments for a STM with performance characteristics superior to ours and conclude that the most reliable way to characterize a surface directionally by STM is to rotate the surface and take a new scan so that only data from the line direction is used for analysis. Another argument for the validity of only considering 2 dimensional line data is that gold tends to form isotropic surface structure. This was reported in virtually all articles cited here. Our analysis involves only 2-d scan lines but conclusions are assumed to be valid for any orientation of a surface.

The algorithm to calculate the radius of curvature consists of three basic steps. First, an interval is chosen over which to compute the radius of curvature. For each data point along the line *n* points to the left and n points to the right are fitted to a parabola so that the length of the fit is $2n+1$ points are fit for each point along the line. *n* is chosen dependent upon the length scale of the line and the amount of noise present. Large *n* act as low pass filtering. The radius of curvature is then computed for the parabola using:

$$\frac{1}{r} = \frac{f''}{(1+(f')^2)^{3/2}} \qquad (10)$$

If the number of points in a line is P, this yields $P-2n$ values of *r* for each line analyzed. Since each scan has different dimensions the data are weighted in real

space. The fitting calculation is detailed in Appendix A.

Figures 17 and 18 represent typical calculations of $1/r$ with this algorithm. The vertical bar on the right gives the scale of the plot of $1/r$. The scales of the scan line are at the bottom, where l=length and h=maximum height variation of the line from peak to peak. Since the calibration of the actuator is not accurate to better than ±20%, only the first significant digit in

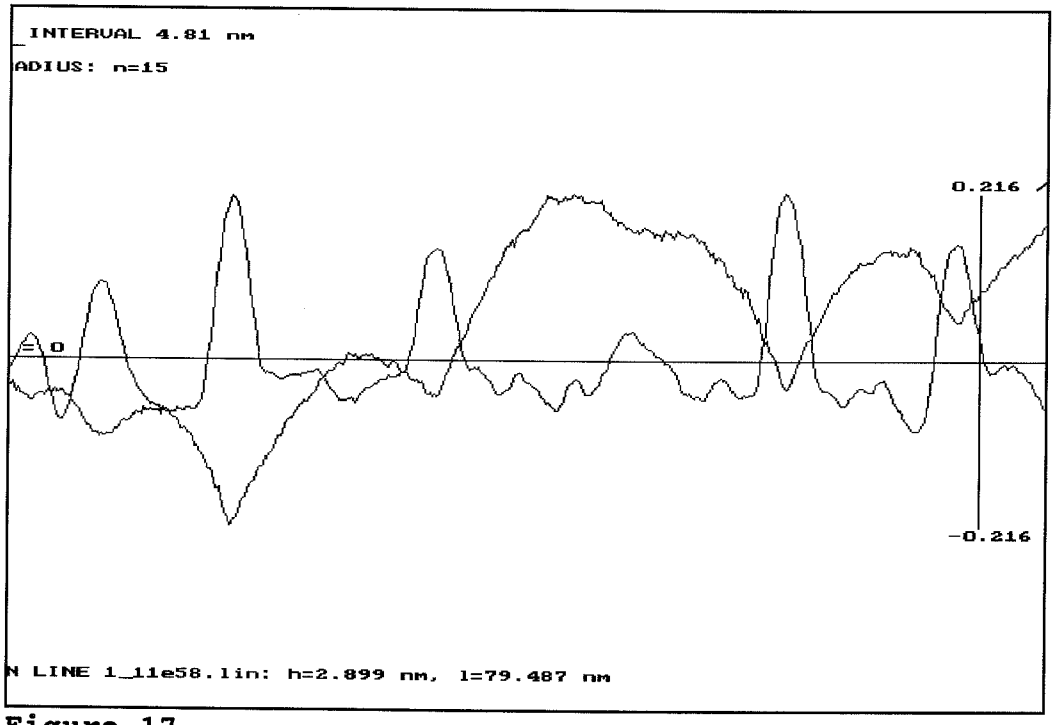

Figure 17

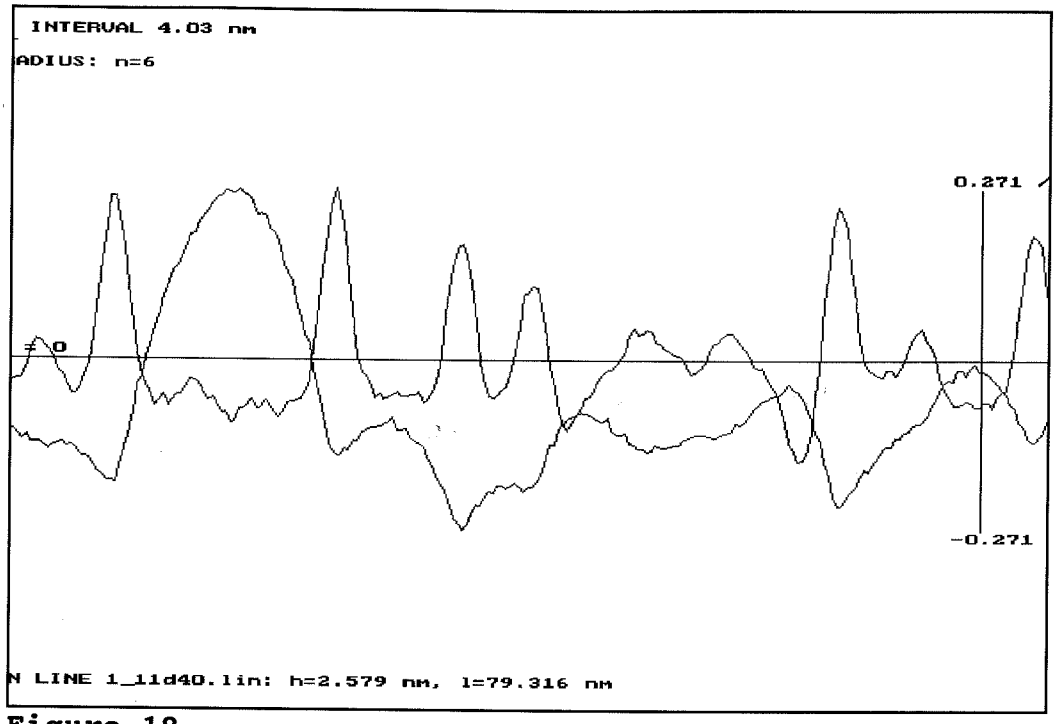

Figure 18

these values should be considered. The value for *n* is given in the upper right. Since each scan has a different length scale and possible a different number of points in it, the size of the interval in real space is also given in nm. The small bar under the word "FIT" gives a visual representation of the length of this interval for comparison with the plot.

Figures 19 and 20 show the effect of different *n* on the analysis. Note that the plots are qualitatively very similar, but, the quantitative values for $1/r$ differ substantially. The peaks representing positive radius of curvature have also widened considerably. From this type

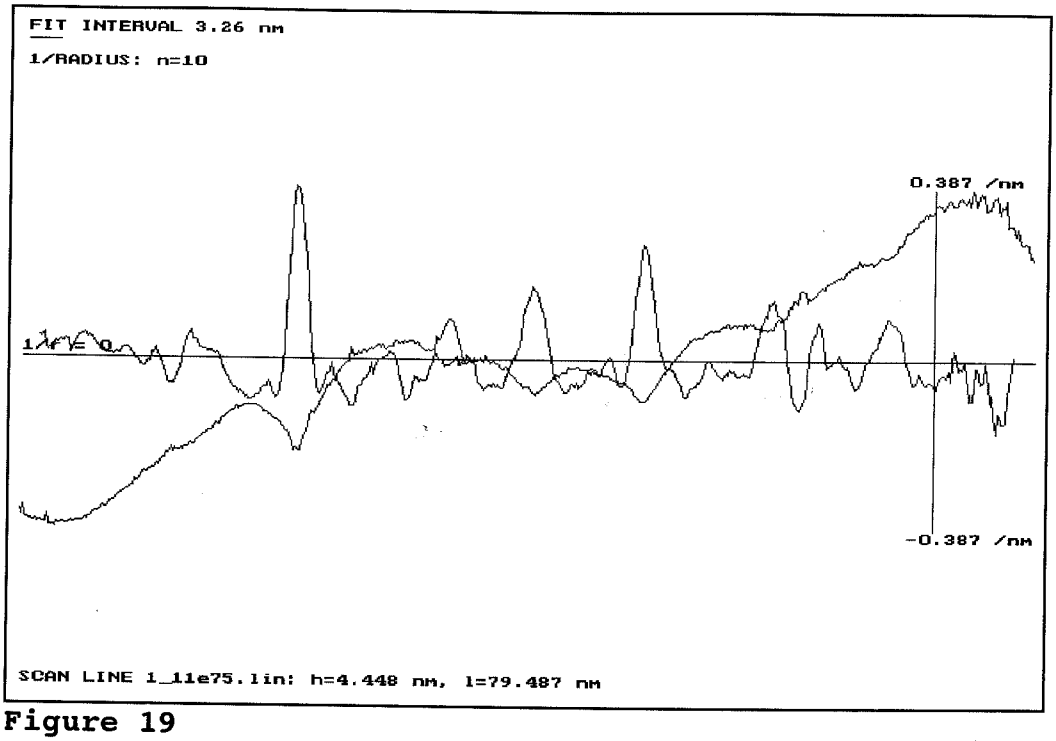

Figure 19

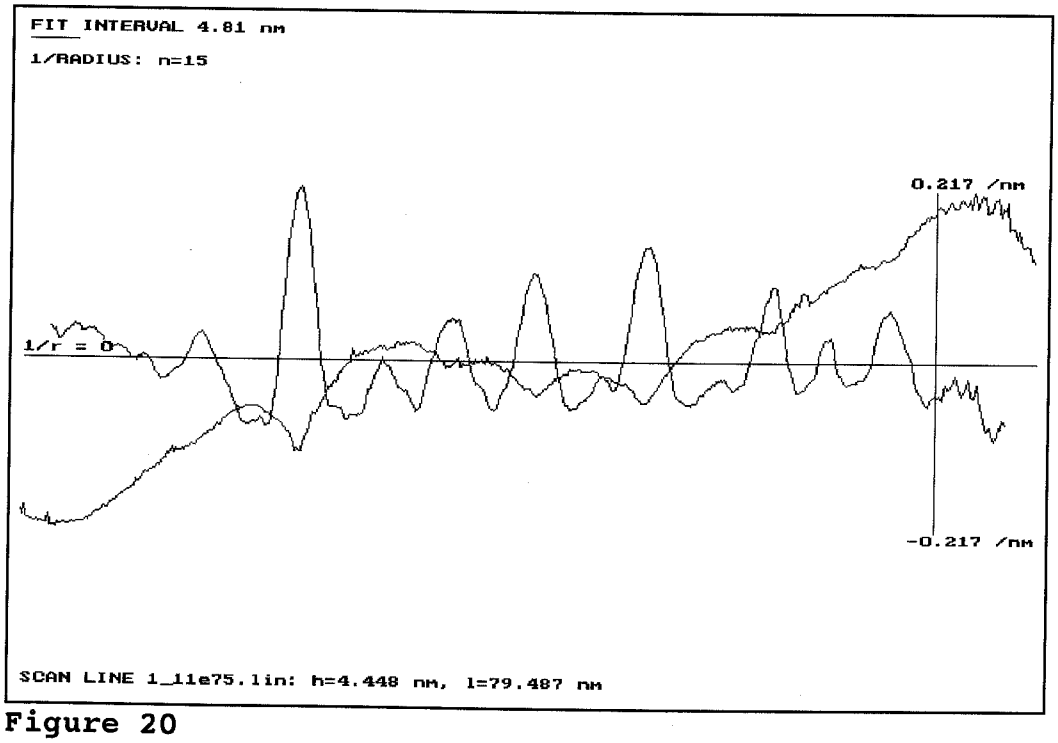

Figure 20

of qualitative information we can assume that if the data

were extremely clean and the fit interval could be made increasingly small that the peaks would approach a delta function.

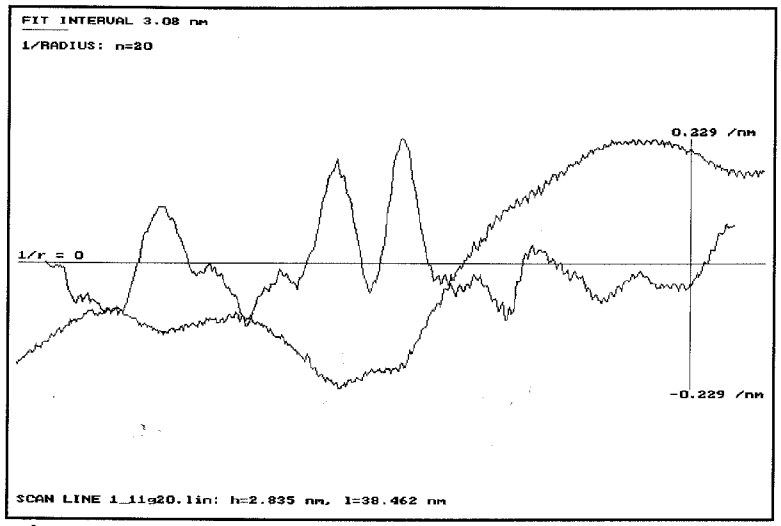

Figure 21

An extreme example of how noise can affect the analysis is shown in Figure 21. The fit interval necessary to smooth out the noise approaches the length of the domes and the values for $1/r$ are only believable over a very small region of the data where the fit interval is not spoiled by crossing a cleft between domes. Other values are too skewed to be considered.

From these data the $1/r$ functions are recorded and a histogram of the function can be made. Figures 22 and 23 show the histograms of $1/r$ for Figures 19 and 20. The curve is fit to a Gaussian distribution as shown in the inset of the graph.

The Gaussian is fit to inverse radius of curvature data less than zero only. This is justified by the same

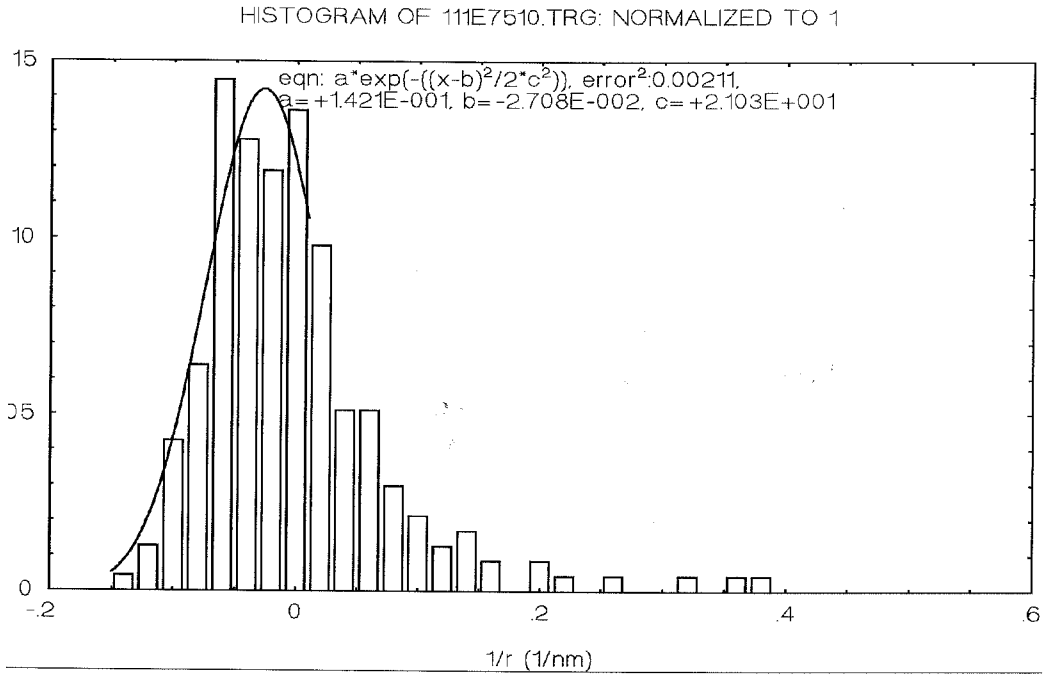

Figure 22

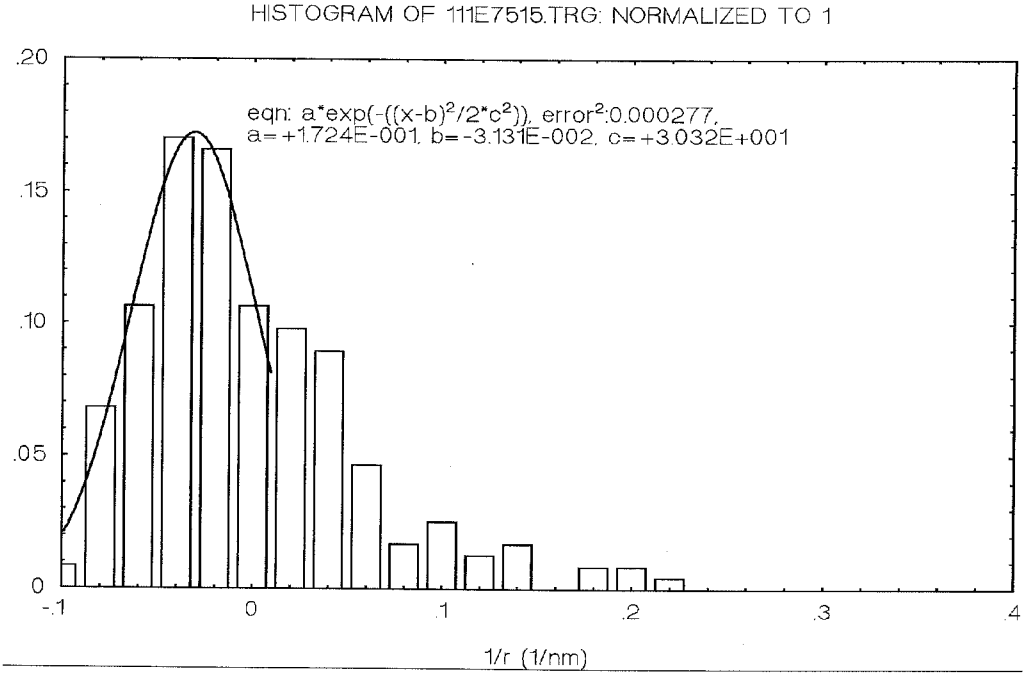

Figure 23

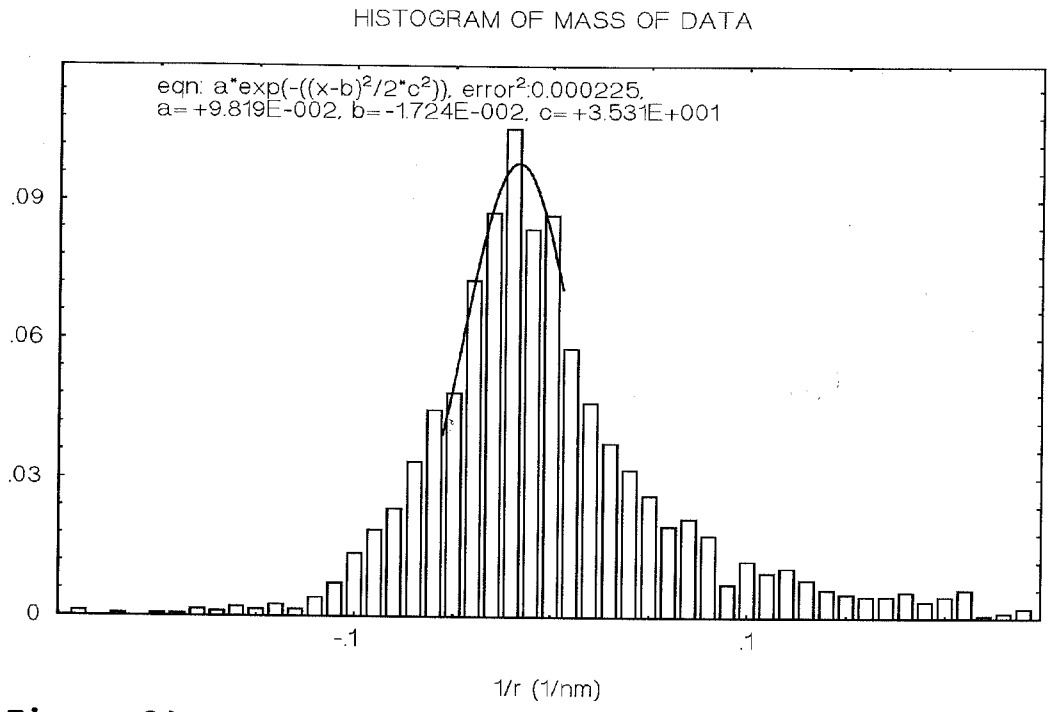

Figure 24

reasoning that the positive peaks should actually be delta functions, they should not enter into the data. The Gaussian fitting equation is of the form

$$G(x) = \frac{1}{\sigma\sqrt{2\pi}} e^{-\frac{(x-x_o)^2}{2\sigma^2}}$$

With the substitutions we have made in our fitting functions

$$a = \frac{1}{\sigma\sqrt{2\pi}} \; ; \quad b = x_o \; ; \quad c = \sigma$$

In order to get general parameters describing the surface as a whole (or at least the part of the surface obeying the "dome" model), many lines from different scan sites were compiled together and statistics were taken.

Figure 24 shows a histogram of the data compiled in the same way that Figures 22 and 23 were compiled.

Data of this type can give us an idea of the distribution of radii of curvature across the surface. The peak of the distribution, x_o, gives the characteristic radius of curvature of the domes, and σ the standard deviation.

One thing that cannot be determined from this analysis is the periodicity of the domes. They may be spherical, but they are only sections of spheres. In order to determine the distribution of the width of the domes the group of data used for Figure 24 was analyzed again. Instead of taking a histogram, a compilation of distances between the positive radius of curvature spikes was made, i.e. the distance between "clefts". These data are shown in Figure 25.

But are these calculations valid? We must be careful when determining both the radius of curvature of the spherical section and breadth of the section. The domes of the surface are arranged randomly. This means that any one scan line probably crosses the apex of at most one of the domes in its path. This would tend to reduce the average measurements of both the radius of curvature and the breadth of the domes. But if we consider the average breadth of domes that we observed versus the radius of curvature we see that the factor is

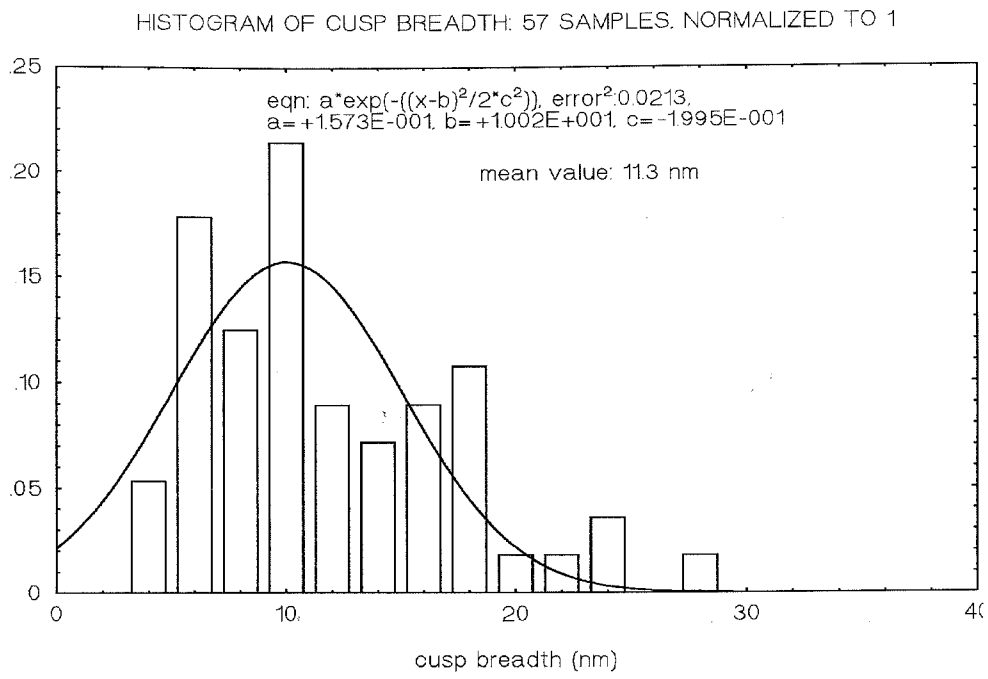

Figure 25

small. If the displacement from the apex of the dome is d and the radius of curvature of the dome r, then the effective radius of curvature measured in a 2 dimensional scan, r_s is given by

$$r_s = r\cos\left(\frac{d}{r}\right)$$

If the worst case is taken where d is large ≈10 nm (1/2 the dome breadth) and r is small, ≈30 nm, then r_s still deviates from r by less than six percent.

From the above analysis we can get a rough idea of the parameters of the spherical dome model of the surface. The distribution of dome breadth in Figure 25 is centered around 10 nm with a geometric mean of 11.3 nm. The inverse radius of curvature distribution in

Figure 24 is centered at 1.7×10^{-2} (the negative sign just means that it is concave down, which we already know), corresponding to an average radius of curvature of ≈60 nm. These Figures coincide well with the observed data. They correspond to an average amplitude of the surface features of 5 nm. Referring to the various one and two dimensional surfaces presented here, which are all scaled, this number is very close to the feature size that we see. These numbers of course, are not independent and so do not verify the validity of our data, but they do verify the validity of the method of analysis.

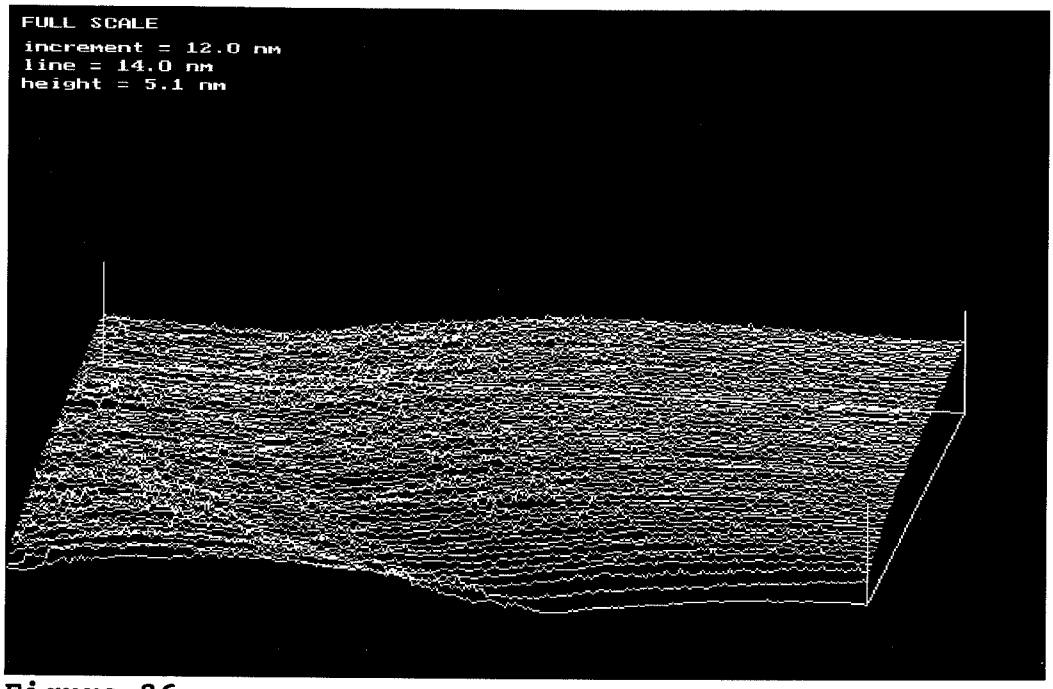

Figure 26

HIGHER RESOLUTION

Many scans of many different sizes were taken during the course of this project. While Professor Ellis' goal was to characterize the surface on the order of nanometers, much smaller scans were often run in hopes of resolving some interesting feature in greater detail. These attempts were most often unsuccessful due to the abundance of vibrational noise at when scanning in air at such high magnification. Two successful scans are shown here. Figure 26 shows a point where two domes come together. The data are too noisy to lend themselves to any numerical analysis of the type used for evaluating

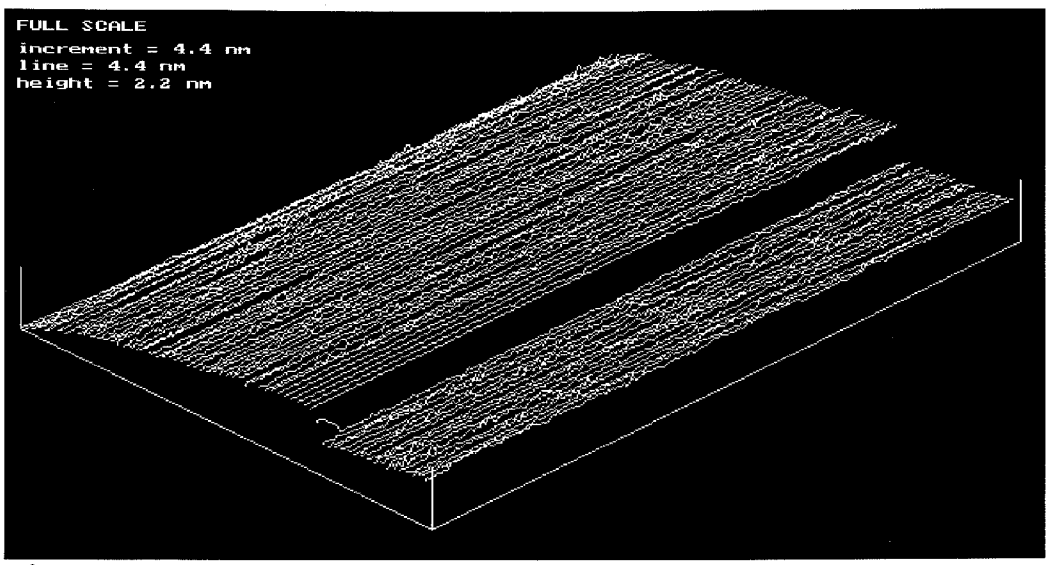

Figure 27

the larger scans.

Figure 27 appears to be even less useful. The large gap in data is caused by readjusting the offset of the high voltage driver while the scan was running. This was often necessary to keep the surface from falling out of range or from crashing the tip. The image appears as noisy as any of the other scans presented here, but the magnification here is much higher. The vertical range is a mere 2 nm and the surface area scanned approximately 20 nm^2. It shows an atomically flat terrace. But given the doubts about the resolution of the STM and all of the concerns about noise, drift, contamination and instability of STM in air, and especially of our experimental apparatus it seems unwarranted to make any conclusion about such a surface.

Several lines from the surface were analyzed in the

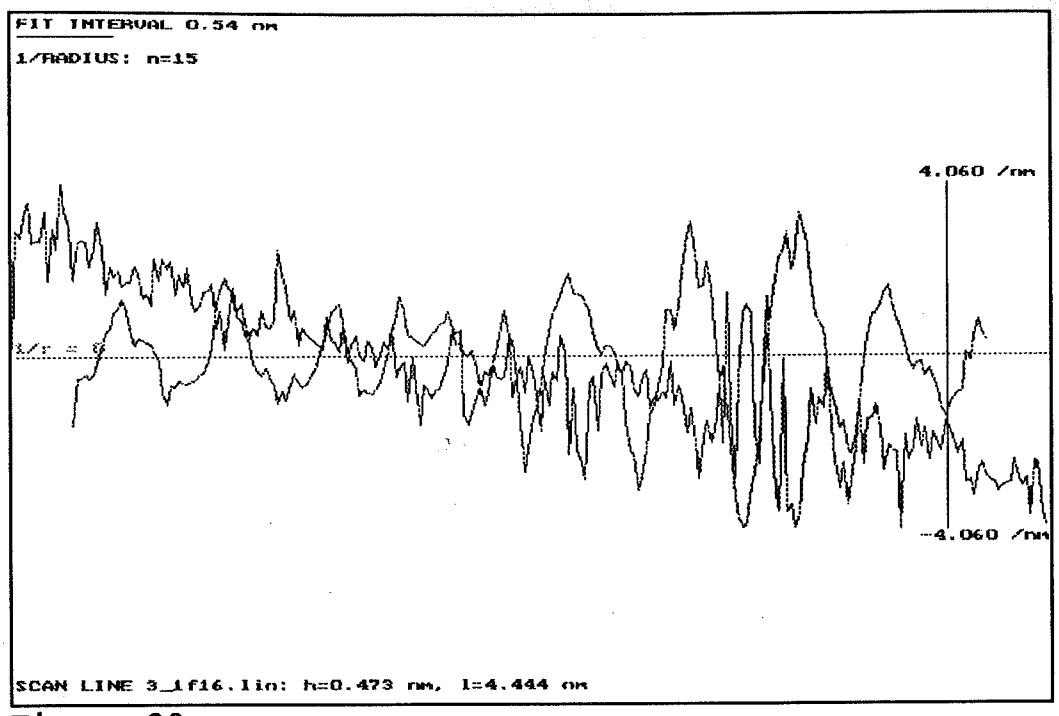

Figure 28

same manner as described above. One of them is shown in Figure 28.

The more erratic line with the overall negative slope is the scan line. Little can be ascertained through the noise. But the peak to peak variation of this line on the screen is only 5 Å, so the noise measures nominally 1 Å. When the inverse radius of curvature is examined it is obvious that there is a very regular, even oscillation between positive and negative radii of curvature. The total length of the line is 4.4 nm (don't forget the large 20% error margin) and there are roughly 10 periods of the oscillation of $1/r$. This gives a separation between maxima and minima of 4.4 Å. The fcc lattice constant for gold has a magnitude of a=4.08 Å[34]

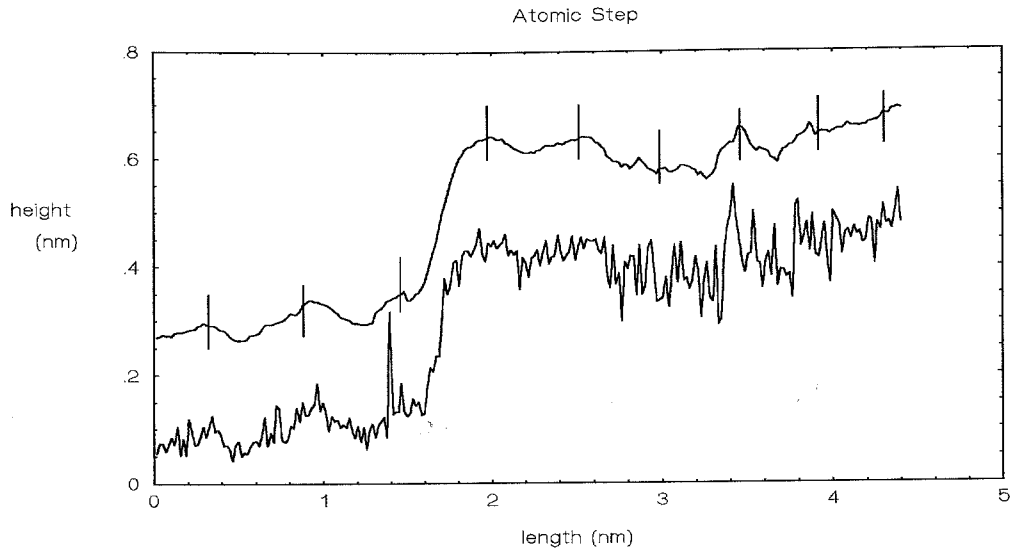

Figure 29

and the surface is assumed to be of the (111) plane orientation. The near neighbor separation should be $d=a/\sqrt{2}=2.9$ Å. From this data I was not able to determine the orientation of the lattice in the image, therefore the lateral response of the actuator can not be definitely determined. If the line is indeed directly along a row of near neighbor atoms then the length of the scan should be roughly 27 Å. This corresponds to a response of the piezoelectric in the Y direction of 21 nm/V.

In the vertical direction it is only necessary to know that the orientation of the surface plane is (111). The atomic step size for this orientation is $h=a/\sqrt{3}$, or 2.35 Å. In Figure 29 just such a step is shown. The lower curve is the original data, the upper curve is a smoothing of the original curve where each point is an

average of 11 adjacent points. The slashes mark atomic centers. The step is ≈3 Å by the present calibration of the vertical response of the actuator. Of course, this is the wrong way of looking at the data. The step *must* be 2.35 Å. Note that the lateral calibration was made from the vertical calibration earlier and the two calibrations are off by a similar factor according to the lattice shown. Regardless of the orientation of the lattice, this STM is conclusively shown to be capable of atomic resolution.

CHAPTER III: CONCLUSION

Part II of this thesis has shown that the STM is capable of operating under the present conditions and of providing valid data. To a certain extent the goal of the STM project has been reached. A characterization of gold surfaces was made that stands up against scrutiny and provides real information useful for calculations necessary for the study of third sound phenomena in superfluid ^{4}He on evaporated gold substrates.

This does not mean that the STM should be put to rest. The conclusions drawn here are only preliminary. The work involved here concentrated primarily on improving the operation of the STM and not on a thorough and systematic study of gold surfaces. This project is one that is ready to produce some interesting and important results. After a review of the literature I believe that an investigation of evaporated gold films on glass is a worthwhile and can definitely lead to publishable results.

Since detailed recommendations on improvement of the STM were given in Part I, I will only summarize my findings here. With the STM now functional its performance can be more scrupulously evaluated. The most immediate problem that needs to be addressed is that of calibration of the lateral motion. If the conclusion

drawn in the last section of Part II concerning the observed atomic corrugations is reliable, and I believe it is, then it should be entirely possible to make such a calibration using an atomic lattice, gold or otherwise.

It is not right to say that obstacles remain since the STM is operational, but it will not provide adequate flexibility until the source of the high gain oscillation problem is identified and rectified. The problems of mechanical coupling, drift, and noise have all been successfully addressed as proven by the resolution shown in the data presented here, but there are still improvements to be made.

Finally, before the STM is developed and improved further some time should be taken to evaluate the system as a whole. There are certainly aspects of the STM that are problematic. The most glaring of them being the great discrepancy between the X and Y responses of the actuator. This could be due to a crack in the piezoelectric or possibly the crosspiece is not polarized properly. It is difficult to determine since the difference has been present from the time it was first calibrated by Firing. I recommend taking the information now available to design the successor to the present STM. This thesis has attempted to build on the knowledge presented by Cahill and Firing and to provide the information necessary for the evaluation of the present

apparatus and design the new one.

APPENDIX A: CURVE FITTING

The radius of curvature algorithm used here involves a very elegant and powerful method of fitting any data to a polynomial. Here I will do it for fitting to a quadratic equation of the form

$$f(x)=ax^2+bx+c \tag{14}$$

If a point along the line of data to be fit is y_o then let the point n points to the left be labeled y_{-n} and the point n points to the right be labeled y_n.

This essentially gives us two equations f(x) and y_i for which we want to minimize the difference over a certain interval. Here we will take the interval from -n to n, which gives us equation 15:

$$\sum_{i=-n}^{n} (y_i-f(i))^2 \Rightarrow minimum \tag{15}$$

For our quadratic equation this sum can be minimized by solving three partial differential equations:

$$\frac{\partial}{\partial a}\sum_{i=-n}^{n} (y_i-(ai^2+bi+c))^2=0 \tag{16}$$

$$\frac{\partial}{\partial b}\sum_{i=-n}^{n} (y_i-(ai^2+bi+c))^2=0 \tag{17}$$

$$\frac{\partial}{\partial c}\sum_{i=-n}^{n}(y_i-(ai^2+bi+c))^2=0 \tag{18}$$

This gives a set of three simultaneous equations for each value of i:

$$\begin{aligned} 2i^2y_i-2ai^4+2bi^3+2ci^2=0 \\ 2iy_i-2ai^3-bi^2+2ci=0 \\ 2y_i+2ai^2+2bi+2c=0 \end{aligned} \tag{19}$$

or

$$\begin{pmatrix} i^4 & i^3 & i^2 \\ i^3 & i^2 & i \\ i^2 & i & 0 \end{pmatrix}\begin{pmatrix} a \\ b \\ c \end{pmatrix} = \begin{pmatrix} i^2y_i \\ iy_i \\ y_i \end{pmatrix} \tag{20}$$

This equation is true for each i, so it must be true for the sum from -n to n. It will be useful to know that:

$$\begin{gathered} \sum_{i=-n}^{n}1=2n+1; \quad \sum_{i=-n}^{n}i=0; \quad \sum_{i=-n}^{n}i^2=2\left(\tfrac{1}{3}n^2+\tfrac{1}{2}n^2+\tfrac{1}{6}n\right); \\ \sum_{i=-n}^{n}i^3=0; \quad \sum_{i=-n}^{n}i^4=2\left(\tfrac{1}{5}n^5+\tfrac{1}{2}n^4+\tfrac{1}{3}-\tfrac{1}{30}n\right); \end{gathered} \tag{21}$$

generalizing equation 20 for the interval of the fit:

$$\begin{pmatrix} \sum_{i=-n}^{n}i^4 & 0 & \sum_{i=-n}^{n}i^2 \\ 0 & \sum_{i=-n}^{n}i^2 & 0 \\ \sum_{i=-n}^{n}i^2 & 0 & \sum_{i=-n}^{n}1 \end{pmatrix}\begin{pmatrix} a \\ b \\ c \end{pmatrix} = \begin{pmatrix} \sum_{i=-n}^{n}i^2y_i \\ \sum_{i=-n}^{n}iy_i \\ \sum_{i=-n}^{n}y_i \end{pmatrix} \tag{22}$$

This equation is solved for *a*, *b*, and *c* in terms of the

various summations:

$$b=\frac{\sum iy_i}{\sum i^2};$$

$$c = \frac{\sum i^4 \sum y_i - \sum i^2 \sum i^2 y_i}{\sum i^4 \sum 1 - \sum i^2 \sum i^2}; \qquad (23)$$

$$a = \frac{\sum i^2 y_i}{\sum i^4} - \frac{\sum i^2}{\sum i^4}\left[\frac{\sum i^4 \sum y_i - \sum i^2 \sum i^2 y_i}{\sum i^4 \sum 1 - \sum i^2 \sum i^2}\right];$$

Since n is chosen before the fit is done, all of the summations which do not include a term for the function being fit, y_i, can be calculated before the fit is performed using equations 21.

This brings us back to the use of the curve fit in this analysis: to find an expression for $1/r$. As stated in Part II, Chapter II, equation 10:

$$\frac{1}{r}=\frac{f''}{(1+(f')^2)^{3/2}}$$

or

$$\frac{1}{r}=\frac{2a}{(1+b^2)^{3/2}} \qquad (24)$$

This equation, however is in some "data space" where 1 data point carries a value of 1 unit. In reality we want this function to be in real nanometer space. This

is accomplished simply by scaling a and b accordingly:

$$a = \frac{a}{\left(\frac{\Delta x}{\Delta i}\right)^2}; \qquad b = \frac{b}{\left(\frac{\Delta x}{\Delta i}\right)}; \tag{25}$$

where $\Delta x/\Delta i$ is simply the distance between data points of the scan line.

ENDNOTES

1. Binnig, Rohrer, Gerber, Wiebel. *Phys. Rev. Left.*, **49** (1): 57 1982.

2. Binnig and Rohrer, *Surface Sci.*, **126**, 237, 1983.

3. Probe microscopes refers to the family of microscopes operating by means of a small tip as opposed to using radiation and lenses. They include the atomic force microscope (AFM) and magnetic force microscopes, the difference being how the tip interacts with the surface.

4. Bill Cahill, B.A. Honors Thesis, Wesleyan University (1992).

5. Jason O. Firing, B.A. Honors Thesis, Wesleyan University (1990).

6. Personal visit at Pennsylvania State University.

7. Binnig, Smith, *Rev. Sci. Instrum.*, **57** (8), 1688 (1986).

8. Ibid.

9. R. Emch, J. Nogami, M.M. Dovek, C.A. Lang, and C.F. Quate, J. Appl. Phys **65** (1), 1989.

10. Schneir, Sonnerfeld, Marti, Hansma, Demuth, Hamers *J. Appl. Phys.*, **63** (3), 717, 1988.

11. Firing, 28.

12. Cahill, 45.

13. Firing, pp. 31-43

14. Ibid, 36.

15. Emch *et al.*, 80.

16. Putnam, Blackford, Jericho, Watanabe, Surface Sci. 217 (1989) 276-288.

17. Firing, 25.

18. Chidsey, Loiacono, Sleator, Nakahara, Surface Sci. 200 (1988) 45-46.

19. Emch *et al.*, 79.

20. Putnam *et al.*, 287.

21. Schneir *et al.*, 717.

22. Emch *et al.*, 80.

23. Emch et al., 82.

24. Chidsey *et al.*, 63.

25. Schneir, Sonnenfeld, Marti, Hansma, Demuth, Hamers, *J. Appl. Phys.* **63** (3): 717, 1 Feb 1988.

26. Blackford, Dahn, Jericho, *Rev. Sci. Instrum.* **58** (8): 1343, August 1987.

27. Mitchell, Bonnell, *J. Mater. Res.* **5** (10): 2244, 1990.

28. Emch *et al.*, 80.

29. Schneir, *et al.*

30. Emch *et al.*, 80.

31. Binnig, Rohrer, *Surface Sci.*, **126**, 243 (1988).

32. Chidsey, *et al.*, 62.

33. Mitchell and Bonnel, 2244.

34. C. Kittel, Introduction to Solid State Physics, New York; Wiley and Sons Inc. 1986, p. 23.